Modeling the Black and Brown Carbon Absorption and Their Radiative Impact: The June 2023 Intense Canadian Boreal Wildfires Case Study

Paolo Tuccella, Ludovico Di Antonio, Andrea Di Muzio, Valentina Colaiuda, Raffaele Lidori, Laurent Menut, Giovanni Pitari, Edoardo Raparelli

JGR Atmospheres

RESEARCH ARTICLE
10.1029/2024JD042674

Modeling the Black and Brown Carbon Absorption and Their Radiative Impact: The June 2023 Intense Canadian Boreal Wildfires Case Study

Paolo Tuccella[1,2], Ludovico Di Antonio[3,4], Andrea Di Muzio[1], Valentina Colaiuda[5], Raffaele Lidori[2], Laurent Menut[6], Giovanni Pitari[1], and Edoardo Raparelli[1,2]

[1]Departement of Physical and Chemical Sciences, University of L'Aquila, L'Aquila, Italy, [2]Center of Excellence in Telesensing of Environment and Model Prediction of Severe Events (CETEMPS), University of L'Aquila, L'Aquila, Italy, [3]University Paris Est Creteil, Université Paris Cité, CNRS, LISA, Créteil, France, [4]Laboratoire, Atmosphères, Observations Spatiales (LATMOS)/IPSL, Sorbonne Université, UVSQ, CNRS, Paris, France, [5]Abruzzo Region Civil Protection Agency, L'Aquila, Italy, [6]LMD/IPSL, École Polytechnique, Institut Polytechnique de Paris, ENS, PSL Research University, Sorbonne Université, CNRS, Palaiseau, France

Key Points:

- Enhanced modeling of black and brown carbon (BrC) improved the simulation of aerosol absorption during the 2023 Canadian wildfires
- Advanced modeling of black and BrC reduced the direct radiative effect of the wildfires by 10%, from −2.1 to −1.9 W/m^2
- Accurate aerosol absorption representation is crucial for predicting the regional climate impact of large-scale biomass burning events

Supporting Information:

Supporting Information may be found in the online version of this article.

Correspondence to:

P. Tuccella,
paolo.tuccella@univaq.it

Citation:

Tuccella, P., Di Antonio, L., Di Muzio, A., Colaiuda, V., Lidori, R., Menut, L., et al. (2025). Modeling the black and brown carbon absorption and their radiative impact: The June 2023 intense Canadian boreal wildfires case study. *Journal of Geophysical Research: Atmospheres*, *130*, e2024JD042674. https://doi.org/10.1029/2024JD042674

Received 17 OCT 2024
Accepted 16 MAR 2025

Author Contributions:

Conceptualization: Paolo Tuccella, Ludovico Di Antonio
Data curation: Paolo Tuccella, Ludovico Di Antonio, Valentina Colaiuda
Formal analysis: Paolo Tuccella, Ludovico Di Antonio, Andrea Di Muzio, Giovanni Pitari
Investigation: Paolo Tuccella, Ludovico Di Antonio
Methodology: Paolo Tuccella, Ludovico Di Antonio
Resources: Raffaele Lidori, Edoardo Raparelli
Software: Paolo Tuccella, Ludovico Di Antonio, Andrea Di Muzio, Laurent Menut

Abstract Black carbon (BC) and brown carbon (BrC) are light-absorbing aerosols with significant climate impacts, but their absorption properties and direct radiative effect (DRE) remain uncertain. We simulated BC and BrC absorption during the intense Canadian boreal wildfires in June 2023 using an enhanced version of CHIMERE chemical and transport model. The study focused on a domain extending from North America to Eastern Europe, including the Arctic up to 85°N. The enhanced model includes an update treatment for BC absorption enhancement and a BrC aging scheme accounting for browning and blanching through oxidation. Validation against Aerosol Robotic Network and satellite data showed the model accurately reproduced aerosol optical depth (AOD) at multiple wavelengths, both near wildfire sources and during transoceanic transport to Europe. Improvements were observed in simulations of absorbing AOD (absorbing aerosol optical) compared with the baseline model. Significant enhancements were achieved in capturing the spatial distribution of aerosol absorption in areas affected by wildfire emissions. For June 2023, the regional all-sky DRE attributed to Canadian wildfires was reduced from −2.1 W/m^2 in the control model to −1.9 W/m^2 in the enhanced model. This corresponded to an additional warming effect of +0.2 W/m^2 (+10%) due to the advanced treatment of BC and BrC absorption. These results indicate the importance of accurate aerosol absorption modeling in regional climate predictions, during large-scale biomass burning events. They also highlight potential overestimations of cooling effects in traditional models, emphasizing the need of improved aerosol parameterization to better simulate the DRE and for evaluating the impacts of mitigation strategies.

Plain Language Summary Black carbon (BC) and brown carbon (BrC) are atmospheric particles that absorb sunlight and contribute to climate warming. BC is emitted from the incomplete combustion of fossil fuels, biomass, and biofuels, while BrC is primarily produced by wood burning. However, their exact climate impact remains uncertain. In this study, we used an improved version of the CHIMERE model to simulate BC and BrC absorption during the intense Canadian wildfires in June 2023. The model covered a vast area from North America to Eastern Europe, including parts of the Arctic. We refined the model to more accurately calculate the BC light absorption and the BrC absorption changes over time (either increasing or decreasing). Comparing the model results with satellite and ground-based data, we found that the updated model more precisely captured the absorption spatial variability, particularly in regions affected by wildfire smoke. The study showed that models lacking proper BC and BrC treatment may overestimate the cooling effect of wildfires. Our improved model reduced the estimated cooling from the 2023 Canadian wildfires by about 10%, emphasizing the importance of accurate modeling to predict the climate impacts of these increasingly frequent events driven by global warming.

1. Introduction

Black carbon (BC) and brown carbon (BrC) are recognized by the scientific community as light-absorbing aerosol particles influencing the climate through the direct (Haywood & Boucher, 2000) and semidirect (Hansen et al., 1997) effects. They darken the surface after deposition on snow and ice packs (Bond et al., 2013; Brown et al., 2022; Flanner et al., 2007; Lin et al., 2014; Tuccella et al., 2021). Additionally, these aerosols can also have

Supervision: Paolo Tuccella
Writing – original draft: Paolo Tuccella, Ludovico Di Antonio
Writing – review & editing: Paolo Tuccella, Ludovico Di Antonio, Andrea Di Muzio, Valentina Colaiuda, Raffaele Lidori, Laurent Menut, Giovanni Pitari, Edoardo Raparelli

indirect effects: acting as cloud condensation nuclei, they can modify cloud optical properties and precipitation patterns. The effects of BC and BrC on the global and regional climate remain uncertain (IPCC, 2021).

BC is formed through the incomplete combustion of fossil fuels (FF), biomass (BB), and biofuels (BF) (Bond et al., 2013). Soot particles exhibit a strong capacity to absorb incoming solar radiation (Bond et al., 2013). Current estimates suggest BC as the third most important contributor to global warming after carbon dioxide (CO_2) and methane (CH_4) (Bond et al., 2013; Gustafsson & Ramanathan, 2016; IPCC, 2021).

BC absorption is influenced by its mixing state (Curci et al., 2019; Tuccella et al., 2020). Mixing state refers to the distribution of chemical and physical properties within an aerosol population (Riemer et al., 2019). In an externally mixed state, different aerosol components exist as separate particles with distinct compositions. Conversely, internally mixed particles within an aerosol population consist of a mixture of chemical species. In the real atmosphere, purely internal or external mixing states are not common (Bondy et al., 2018) and the mixing state continuously evolves due to processes governing the aerosol lifecycle. Freshly emitted BC particles usually have a fractal structure and are externally mixed with non-BC species. After emission, aging processes lead to the formation of internally mixed particles, characterized by a core-shell structure where the BC core is coated by a shell composed of organic and inorganic compounds. The presence of the shell amplifies the BC absorption through the so called "lensing effect" (Jacobson, 2000, 2001; Lesins et al., 2002).

The absorption enhancement (E_{abs}) of coated BC is typically calculated with a Mie theory for the core-shell structure (e.g., Toon & Ackerman, 1981). Several studies have demonstrated that this model is an over-simplification, since it does not consider the complex morphology of BC particles, with implications for absorption calculation (Adachi et al., 2010; Romshoo et al., 2022; Wang et al., 2021). In particular, the core-shell model overestimates the BC absorption enhancement (Adachi et al., 2010; Fierce et al., 2020; D. Liu et al., 2017; Wang et al., 2023).) There is significant variability in reported E_{abs} values, with ambient measurements yielding inconsistent results. Some studies reported significant E_{abs} values, while others found significantly lower values compared with laboratory and modeling simulations (Cappa et al., 2012; Lack et al., 2012; D. Liu et al., 2017). Liu et al. (2017) demonstrated that E_{abs} is influenced by the mass ratio of non-BC to BC. Specifically, BC emitted from urban traffic, characterized by lower non-BC to BC mass ratios, is often better represented as externally mixed with no absorption enhancement. Moreover, the discrepancies between observed and modeled differences have been also attributed to the particle-to-particle heterogeneity in the environment (Fierce et al., 2020; Zeng et al., 2024; G. Zhao et al., 2021). This highlights the importance of incorporating mixing state-dependent absorption parameterizations in atmospheric models to accurately simulate the radiative effects of BC.

Brown carbon (BrC) is defined as the subset of organic aerosol (OA) that exhibits strong absorption (Andreae & Gelencsér, 2006; Laskin et al., 2015) of shortwave radiation with wavelengths less than 400 nm (Lukács et al., 2007; Alexander et al., 2008; Chen & Bond, 2010; Arola et al., 2011; Kirchstetter and Thatcher (2012), Moise et al., 2025). Unlike BC, which shows a weak dependence of absorption with wavelength (λ^{-1}), BrC exhibits a much stronger wavelength dependence, typically ranging from λ^{-2} to λ^{-4} (Laskin et al., 2015). BrC is mainly produced by BF combustion, BB, and aging of secondary organic aerosol|secondary organic aerosols (SOA) (Arola et al., 2011; Bones et al., 2010; Guang-Ming et al., 2016; Hecobian et al., 2010; Lambe et al., 2013; Laskin et al., 2015; Lee et al., 2014; Updyke et al., 2012). Other sources are likely related to the secondary BrC formation in cloud liquid water (Guo et al., 2022; Hems et al., 2021; Zhang et al., 2017). The representation of OA optical properties in climate models has evolved over the past decade. From being considered as scattering particles, the BrC absorption is now included in many global (Brown et al., 2018; DeLessio et al., 2024; Drugé et al., 2022; Feng et al., 2013; Jo et al., 2016; Lin et al., 2014; Saleh et al., 2015; Tuccella et al., 2020, 2021; Wang, Heald, et al. (2014), Wang, Zhang, et al. (2014), 2018; A. Zhang et al., 2020) and regional modeling studies (Konovalov et al., 2024; Methymaki et al., 2023; Park et al., 2010; Skyllakou et al., 2024; Xu et al., 2024).

Primary BrC absorption is not constant over time but varies with aging processes that OA undergoes. Experimental results have suggested that BrC optical properties may be modified through aqueous-phase photochemical reactions, potentially leading to both photo-enhancement and photobleaching (R. Zhao et al., 2015). The increase of BrC absorption is called "browning" and it is primarily driven by heterogeneous oxidation reactions with hydroxyl (OH) and nitrate (NO_3) radicals, as well as aqueous oxidation (Cheng et al., 2020; Hems et al., 2020; Schnitzler et al., 2020). Following browning, primary BB BrC undergoes bleaching, a process attributed to oxidation by OH and ozone (O_3) (Hems et al., 2021).

While photobleaching is frequently incorporated into models simulating BrC (Brown et al., 2018; Drugé et al., 2022; Wang et al., 2018; A. Zhang et al., 2020), browning is often overlooked. To our knowledge, only DeLessio et al. (2024) have accounted for photo-enhancement in their study. The same authors concluded that accurate representation of the diurnal variability in OA absorption necessitates the inclusion of the browning process in the atmospheric models.

Many studies have demonstrated that wildfires impact the climate system (Eckdahl et al., 2022; Li et al., 2017; Linares & Ni-Meister, 2024; Randerson et al., 2006; Walker et al., 2018). At the same time, the frequency of wildfire events is increasing due to climate warming. The relationship between climate change and wildfire frequency has been studied since the early 1990s (van Bellen et al., 2010). The Arctic is warming at more than twice the global average rate (Meredith et al., 2019), which contributes to the rise of wildfire activity in boreal regions of Alaska and western Canada (Gillett, 2004; Veraverbeke et al., 2017). Moreover, the Northern Hemisphere has experienced extreme wildfire seasons, as for example, the 2023 Canadian events (Byrne et al., 2024), leading to significant aerosol emissions, with notable impacts on aerosol properties even in Europe (Filonchyk & Peterson, 2024). Additionally, in the future, anthropogenic aerosol mitigation could be a significant driver in enhancing boreal forest fires, due to a deeper layer of soil drying during the summer, driven by increased surface solar radiation and enhanced evapotranspiration (Allen et al., 2024).

Boreal forest fires are important sources of BC and OA, which may exert significant regional climate feedback at regional scale (Konovalov et al., 2024; Konovalov and Golovushkin (2024)). Accurate simulation of BC and OA absorption properties is essential for estimating the climatic impact of boreal wildfires.

This study provides a comprehensive assessment of BC and BrC absorption during the 2023 Canadian boreal wildfires using an enhanced parameterization within the CHIMERE chemical and transport model. The results underscore the critical role of aerosol absorption modeling for an accurate simulation of the regional direct radiative effect (DRE), associated to large-scale wildfire events. In Section 2, we detailed the model description and setup, where we included a treatment for improving the BC absorption and a treatment for BrC absorption, including an update parameterization for BC E_{abs} and a treatment for BrC absorption, accounting for both browning and blanching processes. In Section 3, the simulated optical properties have been evaluated against satellite and ground-based observations, including data from Moderate Resolution Imaging Spectroradiometer (MODIS), the Ozone Monitoring Instrument (OMI) Aura Near UV OMAERUV, and the Aerosol Robotic Network (AERONET). Finally, in Section 4, we discussed the DRE of the June 2023 Canadian smoke aerosol.

2. Methods

2.1. CHIMERE Model Description and Setup

In this study, we have used the 2021 version of the CHIMERE model (Menut et al., 2021) to simulate the absorption of BC and BrC, coupled online with the meteorological Weather Research and Forecasting (WRF) model. This online configuration is capable to simulate both direct (Briant et al., 2017) and indirect aerosol effects (Tuccella et al., 2019). The WRF model is a mesoscale meteorological model including several parameterizations for atmospheric processes (https://www.mmm.ucar.edu/models/wrf, last access: 09 October 2024). CHIMERE is a chemical and transport model suitable for studies ranging from hemispheric to urban scales (Mailler et al., 2017). It contains multiple numerical schemes for simulating the gas-phase and aerosol processes. Weather Research and Forecasting and CHIMERE are coupled with the external coupler OASIS3-MCT (Craig et al., 2017). The information between models is exchanged with a regular frequency defined by the user (Briant et al., 2017).

We simulated the entire month of June 2023, after a one-month of spin-up for chemistry. WRF-CHIMERE was configured on the domain shown in Figure 1. This domains spans from North America to Eastern Europe, in latitude it extends from Tropics up to North Pole. The horizontal resolution was of 78 km, with 190 × 127 grid points. We used 33 vertical levels extending from surface up to 50 hPa for WRF, and 30 levels up to 200 hPa for CHIMERE. The coupling time (i.e., exchange frequency) between WRF and CHIMERE was fixed at 20 min.

Main schemes adopted for WRF are the Yonsei University for planetary boundary layer (Hong et al., 2006), NOAH as land surface model (Chen & Dudhia, 2001), RRTMG for shortwave and longwave radiation (Iacono et al., 2008), Thompson for cloud microphysics (Thompson et al., 2008), and Grell-Freitas scheme for cumulus convection (Grell & Freitas, 2014). In CHIMERE, gas-phase reactions were calculated with the MELCHIOR2

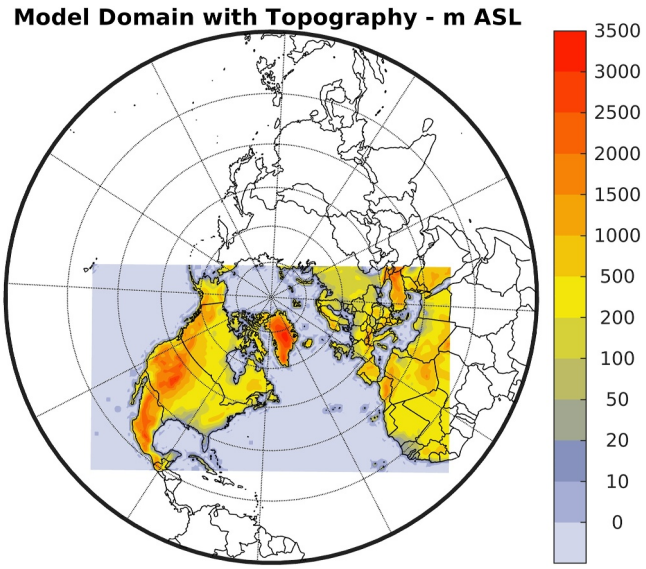

Figure 1. The domain used to run WRF-CHIMERE The colors represent the altitude above sea level of the model topography. The grid had horizontal resolution of 78 km with 189 × 109 grid points.

model (Derognat et al., 2003), which includes 40 gaseous species and 120 photochemical reactions. Photolytic rates were parameterized with the FAST-JX model (Wild et al., 2000), as detailed in Mailler et al. (2016, 2017). Aerosol treatment is based on a sectional approach (Bessagnet et al., 2008; Mailler et al., 2017). Here, we have used 10 dimensional bins ranging from 0.01 up to 40 µm. Aerosol model includes the main inorganic species (sulfate, nitrate, ammonium), water, BC, primary organic aerosol (POA), unspeciated particles (which include primary particulate matter that is neither POA nor BC), SOA, sea salt, and soil dust. We simulated anthropogenic and biogenic SOA with a single-step oxidation scheme, according to Bessagnet et al. (2008). Anthropogenic SOA precursors include toluene, trimethylbenzene, and higher alkanes, while biogenic SOA precursors are terpenes, α-pinene, β-pinene, and limonene. Thermodynamic equilibrium of inorganic aerosols was simulated by using the ISORROPIA model (Nenes et al. (1998)). Dry deposition of gases and aerosols were calculated with the schemes proposed by Wesely (1989) and Zhang et al. (2001), respectively. Wet deposition calculation followed the methods of Wang, Heald, et al. (2014), Wang, Zhang, et al. (2014), as detailed in Mailler et al. (2017).

Aerosol optical properties in CHIMERE are calculated under the assumption of external mixing state, as outlined in Mailler et al. (2017), at 200, 300, 400, 600, and 999 nm. Extinction efficiency, single scattering albedo (SSA), and asymmetry parameter are first determined for each aerosol particle type across each dimensional bin and are then summed to obtain the total values for each optical property. These optical parameters are calculated assuming the aerosol particles as spherical using the Mie theory (Mie, 1908), solved through the spher. f code (Mischenko et al., 2002). Most of the aerosol complex refractive indices adopted in CHIMERE are based on the ADIENT project (Mailler et al., 2016), with exception of BrC and BC. These latter are discussed in Sections 2.2 and 2.3.

Anthropogenic emissions of trace gases and particles were taken from Copernicus Atmosphere Monitoring Service (CAMS) global inventory (Soulie et al., 2024) for the year 2022. Biomass burning emission fluxes were obtained from the CAMS data set as described by Kaiser et al. (2012). Both inventories are at horizontal resolution of 0.1° × 0.1° and were re-gridded onto model grid according to Menut et al. (2021). Forest fire emissions from CAMS relative to June 2023 are displayed in Figure 2. Vertical injection profile of fire emissions adopted in CHIMERE is described in Menut et al. (2018). The injection height is calculated as in Sofiev et al. (2012) and corrected according to Veira et al. (2015), in case of huge fire. After the estimation of injection height, the shape of injection profile was calculated with the so called $2K_z$-like shape, where the emissions profile presents two maxima, one close to surface and one around injection height. Soil dust emissions were computed by using the scheme developed by Alfaro and Gomes (2001), with optimizations introduced by Menut et al. (2005). Sea salt emissions were estimated in accordance with Monahan (1986). NO_x emissions by lightning were included using the scheme of Price and Rind (1993), as detailed by Menut et al. (2020). Biogenic emissions were considered in our simulations employing the version 2.04 of MEGAN model (Guenther et al., 2012).

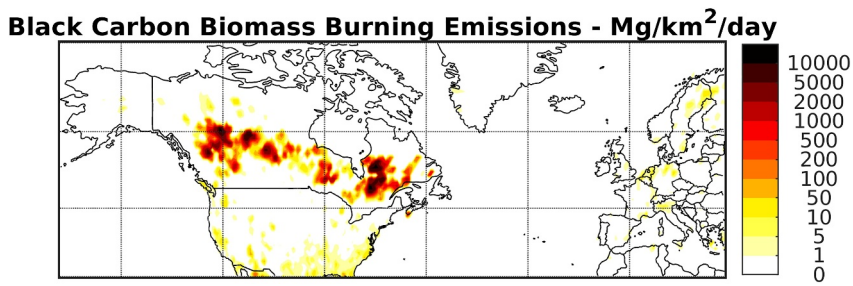

Figure 2. Biomass burning (BB) emission flux of black carbon during the month of June 2023 obtained from the Copernicus Atmosphere Monitoring Service database.

Initial and boundary conditions for WRF were obtained from 6-hourly National Centers for Environmental Prediction (NCEP) operational analyses at resolution a of 1° × 1°. Grid nudging toward NCEP analysis data of wind, temperature, and water vapor was applied in WRF on the model vertical levels above the planetary boundary layer. Sea ice extent and sea surface temperature were taken from NCEP data and were updated every 6 hours. CHIMERE was driven by the boundary conditions derived from the 2010–2017 gas and aerosol climatology based on the Laboratoire de Météorologie Dynamique Zoom-INteraction with Chemistry and Aerosols global model (Folberth et al., 2006).

2.2. BC Treatment

Within CHIMERE, the aerosol optical properties are calculated assuming an external mixing approach, which does not account for the BC absorption enhancement due to the lensing effect associated with the core-shell morphology of coated BC. Consequently, we have implemented within CHIMERE a scheme to account for this effect, drawing on the work of Liu et al. (2017). The authors demonstrated that E_{abs} depends on the mass ratio (M_r) of BC, given by ratio between the mass of non-BC aerosols and mass of soot particles. When $M_r < 1$, BC is external mixed and absorption enhancement is not observed ($E_{abs} = 1$). For $M_r > 3$, Liu et al. (2017) suggest that E_{abs} is captured by the core-shell model as BC is internally mixed and positioned at the center of a non-BC coating. When M_r is between 1 and 3, a transitional regime is observed, and only one fraction of BC is internally mixed, while the remaining part is externally mixed. Therefore, for small M_r typical of fresh traffic sources (less than 1.5), E_{abs} is small (Schwarz et al., 2008). In fact, an E_{abs} of 1.1 has been reported in urban regions of California (Cappa et al., 2012) and China (Lan et al., 2013). When M_r is larger (greater than 3), as for example, in BB emissions, E_{abs} is in the range of 1.3–1.9 (Kompalli et al., 2023; Lack et al., 2012; Rathod et al., 2021).

Therefore, E_{abs} has been parameterized with the hybrid optical model of Liu et al. (2017). In this approach, no E_{abs} occurs when $M_r < 1$ and is linearly interpolated to the upper threshold of $M_r = 3$, for $M_r > 3$ E_{abs} is accurately predicted by core-shell model:

$$E_{abs} = E_{abs_{cs}} F_{in} + (1 - F_{in})$$

with

$$F_{in} = 0 \quad \text{for } M_r \leq 1.5$$

$$F_{in} = 0.57 M_r - 0.74 \quad \text{for } 1.5 < M_r \leq 3$$

$$F_{in} = 1 \quad \text{for } M_r > 3$$

where $E_{abs_{cs}}$ is the absorption enhancement calculated by core-shell model and F_{in} is the internally mixed fraction of BC. $E_{abs_{cs}}$ should be estimated with a core-shell algorithm; however, in this study, we used a constant value of 1.5. We have chosen this value because it is representative of the mean of E_{abs} estimations (Kong et al., 2024), which coincides with the average value recommended by Bond and Bergstrom (2006). It should be noted that the 90% confidence interval of E_{abs} distribution function reported by Kong et al. (2024) ranges from 1.15 (5%) to 2.18 (95%). This highlights that BC absorption simulation may depend on the value of $E_{abs_{cs}}$ adopted. Finally, the refractive index assigned to BC was 1.95–0.79i, as recommended by Bond and Bergstrom (2006). Although this value is used in many atmospheric models, it may be overestimated as also mentioned by the same Bond and Bergstrom (2006). This result is highlighted also in Brown et al. (2021) through multimodel simulations of BB absorption properties.

2.3. BrC Treatment

The CHIMERE model treats OA only as scattering aerosol particles. Therefore, we have implemented a scheme to consider the BrC absorption within CHIMERE simulations. To our knowledge, currently there are not emission inventories of BrC. Previously, different methods have been employed to estimate the primary BrC emissions. For example, Jo et al. (2016) derived BrC emissions fluxes using a relationship between the modified combustion efficiency and absorbing Ångström exponent. Other studies, such as Feng et al. (2013) and Wang, Heald,

et al. (2014), Wang, Zhang, et al. (2014), have assumed that a fraction of emitted OA was BrC. Additionally, emissions have been also inferred from BC-to-OA ratio (Brown et al., 2018; Neyestani & Rawad Saleh, 2022; Park et al., 2010; Saleh et al., 2015; A. Zhang et al., 2020). Alternatively, other researchers have treated all OA as radiation-absorbing particles, assigning to them specific optical properties (Wang et al., 2018). In our investigation, we have used this latter approach, as detailed below.

In our model, we consider the OA emitted from wildfires and biofuel as primary sources of BrC. For clarity, emissions from forest fires are referred to as biomass burning BrC (BB-BrC), while emissions from biofuel use are termed biofuel BrC (BF-BrC) throughout the study. Consequently, we have partitioned primary OA into three distinct tracers: fossil fuel, biofuel, and BB, which have been incorporated into the CHIMERE model.

BB-BrC emissions were taken directly from forest fire CAMS emission inventory (see Section 2.1). By contrast, BF-BrC emissions have been estimated from anthropogenic emission fluxes from domestic, industrial, waste management, and agricultural sectors. Specifically, a fraction of these emissions was considered as BrC. This portion was derived based on the ratio of BF emissions to the total anthropogenic (FF + BF) OA emissions, as reported in the inventory of Bond et al. (2007), and then applied to the OA anthropogenic emissions from CAMS, after being treated as described in Section 2.1.

In this investigation, we utilized the BrC optical properties as suggested by Wang et al. (2018), which were obtained constraining the mass absorption coefficient (MAC) of BB BrC with measurements from aircraft campaigns conducted in the continental United States. Additionally, the same authors demonstrated that their optical properties were applicable to reproduce the BB-BrC absorption observed over Europe. Consequently, we have adopted the MAC values from Wang et al. (2018), since our study is focusing on North America and Europe. Additionally, in our prior investigations, we were able to calculate BrC absorption at global scale in the atmosphere (Tuccella et al., 2020) and within snow (Tuccella et al., 2021), using this set of optical properties. MACs at 365, 440, and 550 nm were 1.19, 0.76, and 0.39 m^2/g for BF-BrC, and 1.33, 0.77, and 0.35 m^2/g for freshly emitted BB-BrC, respectively.

Photochemical aging of BB-OA is crucial in simulating BrC absorption, since it induces blanching of BrC through photochemistry processes. Several methodologies have been adopted to simulate the BB-BrC aging. One of these consists in the passage from hydrophobic to hydrophilic, with hydrophilic component exhibiting a lower absorption compared with its hydrophobic counterpart (e.g., Drugé et al., 2022; Tuccella et al., 2020; A. Zhang et al., 2020). The transition is usually done with a characteristic time scale. Alternatively, some studies have adopted a blanching scheme where the absorption was tracked and attenuated based on OH concentration and a characteristic half-life time scale (Brown et al., 2018; Wang et al., 2018). However, the most recent advancement in BB-BrC aging modeling has been introduced by DeLessio et al. (2024). This consists in considering the heterogeneous oxidation of BB-BrC by hydroxyl radical (OH), nitrate radical (NO_3), and ozone (O_3), according to the results of Hems et al. (2021). This innovative approach has been adopted and integrated in our investigation.

Specifically, following DeLessio et al. (2024), the aging processes was divided in two distinct steps. In the first, freshly emitted BB-BrC undergoes an absorption enhancement, a phenomenon known as "browning". In the second phase, the "browner" BrC is subjected to blanching process, during which the absorption is lower than that of freshly emitted BrC. Transfer mass from freshly emitted BrC to more absorbing BrC is succeeded by whitening, involving mass transfer from browner to less absorbing BrC. The mass transfer was quantified with second order rate constant for each reaction of BB-BrC with OH, NO_3, and O_3. During the nighttime, freshly emitted BB-BrC is oxidized by NO_3 to form more absorbing OA, which then becomes less absorbing through subsequent oxidation with O_3. During daylight hours, freshly BB-BrC is oxidized by OH to form more absorbing BrC. This browner BrC is then blanched through oxidation with OH and O_3. Rate constants used were the same of DeLessio et al. (2024), derived from the initial first reaction rate for BrC processing defined by Hems et al. (2021), with oxidant concentrations assumed by same authors.

The MACs at 365, 440, and 550 nm of less absorbing BB-BrC were set at 0.37, 0.23, and 0.10 m^2/g, respectively (Wang et al., 2018). These values reflect the average absorption of BB BrC and are recommended for applications in models where absorption is not tracked. They should be used to account for absorption reduction when the whitening is not explicitly simulated (Wang et al., 2018). We note that the MACs adopted for less absorbing BB-BrC were slightly less 30% of those of freshly emitted OA. However, this value is very close to the minimum threshold of ¼, imposed by the same authors (Wang et al., 2018), below which the absorption may not drop, when

Table 1
Summary of the Numerical Experiments

Simulation	Description
CTRL	Control simulation. Default model.
BC_{Eabs}	Only BC absorption enhancement
BEST	BC absorption enhancement and BrC absorption
H-ABS	High absorption scenario: E_{absCS} = 1.9, no BB-BrC aging
L-ABS	Low absorption scenario: E_{absCS} = 1.2, all BB-BrC is aged

it is tracked to account for BrC blanching. In addition, this value is also close to threshold of 20% based on laboratory studies (Fleming et al., 2020; Hems et al., 2021). As in DeLessio et al. (2024), we assigned to browner BB BrC a MAC that is 150% larger of that attributed to freshly emitted OA.

The MAC values adopted for BrC, along with the corresponding imaginary parts of the refractive indices, are detailed in Tables S1 and S2 in Supporting Information S1. These MAC values at 365, 440, and 550 nm were interpolated onto the CHIMERE wavelengths using the absorbing Ångström exponent (absorbing angström exponent). These values were of 3.3 for BB-BrC and 2.7 for BF-BrC.

In this work, we have also assumed that both biogenic and anthropogenic SOA are absorbing. We attributed to SOA-BrC the same set of optical properties of Wang et al. (2014a, 2014b), that for a typical size distribution of organic aerosols result in a MAC of 0.3 m^2/g at 440 nm.

2.4. Numerical Simulations

We performed a series of model simulation to evaluate the model development described above. The list of our runs is reported in Table 1. The first simulation has been conducted with the default version of CHIMERE, which does not include the BC absorption enhancement and BrC effects. This reference simulation (control, CTRL) was used to evaluate the aerosol transport and basic skill of the model in reproducing the aerosol optical depth (AOD) distribution. This choice was justified since the AOD differences between the reference run and the enhanced simulations, described below, are negligible. The second simulation included only the scheme for BC_{Eabs} and was aimed to evaluate how this parameterization improves the aerosol absorption simulation in CHIMERE (BC_{Eabs}). The third run takes into account both BC E_{abs} and BrC absorption. This simulation was labeled as "BEST" as it includes all the parameterizations introduced to enhance CHIMERE and because it represents a central estimate of absorption compared with the perturbed runs described below.

Other two simulations have been conducted to estimate the sensitivity of BC and BrC absorption to aerosol optical properties uncertainties. Consequently, we created a high absorption scenario (H-ABS) and a low absorption scenario (L-ABS), perturbing the BEST run. In the first case, we have not considered the BB-BrC aging assigning it the MAC of freshly emitted BB-OA. Furthermore, $E_{abs_{cs}}$ was set to 1.9, representing the 90th percentile of E_{abs} distribution (Kong et al., 2024). By contrast, in the L-ABS scenario, we assigned to BB-BrC the MAC of blanched OA and $E_{abs_{cs}}$ was set to the 10th percentile of E_{abs} distribution reported in Kong et al. (2024), which is equal to 1.2. Consequently, by considering these two extreme cases of absorption, we have evaluated the sensitive of carbonaceous aerosols absorption, associated to uncertainties of BC absorption enhancement and BrC aging parameterizations.

All simulations were conducted without the direct and indirect radiative effects, since they may introduce feedback mechanisms that could influence atmospheric dynamics and subsequently affect the evaluation of model updates. Furthermore, the primary objective of this study is to assess the DRE of the 2023 Canadian wildfire episode and to investigate the implications of model development on its estimation. The activation of direct and indirect effects could further alter the radiation budget through modifications in cloud coverage and properties. However, this is a subject that deserves future investigation.

2.5. Evaluation Strategy

Numerical simulations have been compared with aerosol optical properties retrieved from ground-based and satellite instruments. Before the comparison, the CHIMERE output was regridded onto a regular grid with a horizontal resolution of 0.7° × 0.7°. The regular domain is presented in Figure 3.

Ground-based observations were taken from the version 3 of AERONET sun- and sky-scanning radiometers (Holben et al., 2001; Sinyuk et al., 2020). AERONET is a global network providing observations of spectral columnar aerosol optical properties, such as AOD, absorbing aerosol optical depth|absorption aerosol optical depth (AAOD), and SSA, at 440, 675, 870, and 1,020 nm. AERONET disseminates data according to different quality check criteria: the cloud-screened L1.5, and cloud-screened and quality-assured (QA) L2.0 (Dubovik et al., 2002). In the latter, SSA is provided only when AOD levels at 440 nm exceeds 0.4. Consequently, only 18%

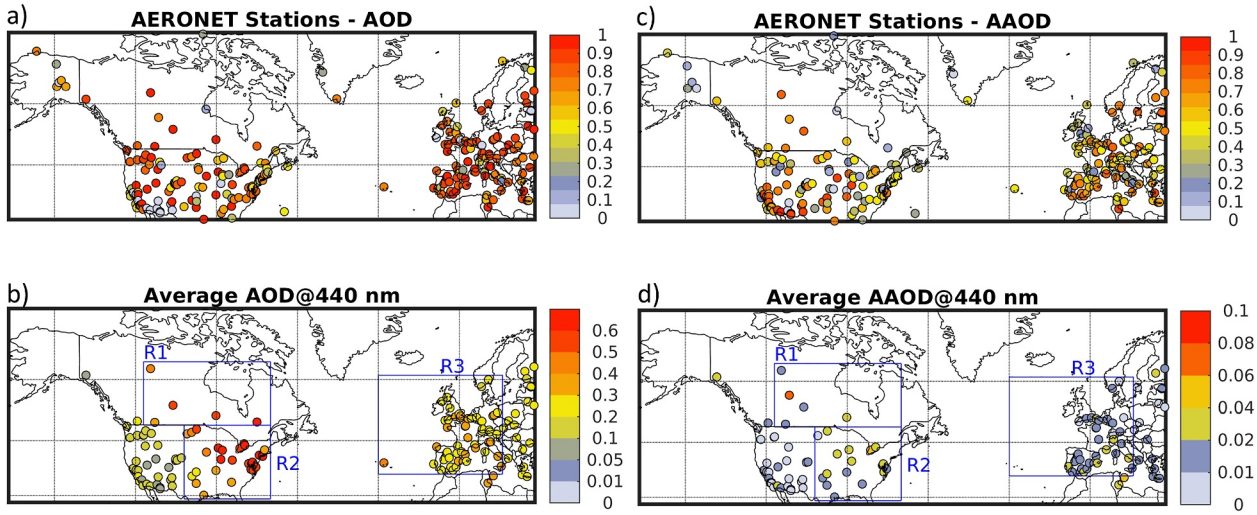

Figure 3. Aerosol Robotic Network (AERONET) stations used to evaluate the model simulations. The color scale represents the fraction of data coverage (see Section 2.5) in June 2023 for the aerosol optical depth (AOD) (a) and the absorbing aerosol optical depthlabsorption aerosol optical depth (AAOD) (c), and the mean AOD (b) and AAOD (d) at 440 nm measured at AERONET sites. Average AOD is calculated at the stations with at least 75% of monthly data coverage, while monthly AAOD is calculated at sites with at least 55% of data coverage. The regions R1, R2, and R3 outlined by blue rectangles indicate the area most affected by Canadian boreal fires (see Section 2.5).

of L2.0 data available in June 2023 was AAOD. Thus, following the methodology used in our previous studies (Curci et al., 2019; Tuccella et al., 2020), based on the work of Wang et al. (2016), we have complemented the L2 AAOD data with the L1.5.

Figure 3 displays the AERONET sites available during our study period, along with the fraction of AOD data availability for each site in June 2023. This fraction is calculated as the ratio between the number of daily observations (averaged from the available data for each day) and the 30 days of the month. For our analysis, we included only the stations with at least 75% of data availability. Figure 3 also illustrates the average AOD at 440 nm measured at these sites during June 2023. Based on these AOD values, we identified three regions that were most impacted by Canadian forest fires, which are outlined with blue rectangles in Figure 3. The first region (R1) included the AERONET stations located in Canada, representative of the measurement sites directly affected by the boreal fire sources. The second region (R2) covered the Eastern USA, where the observation stations were affected by smoke transported downwind the fire sources. Finally, the third region (R3) was represented by Western Europe, where AERONET sun photometers were subjected to transoceanic transport of Canadian boreal wildfire aerosols. In these three regions, we conducted a thorough and detailed analysis of the model performances. The AERONET stations used for AAOD evaluation are also displayed in Figure 3. In our analysis, we included only the stations with at least 55% of data availability, due to the reduced availability of AAOD data compared with AOD.

The simulated monthly spatial AOD pattern at 550 nm was compared with the MODIS AQUA data (Levy and Hsu, 2015). In this work, we used the "AOD_550_Dark_Target_Deep_Blue_Combined" merged product from the "MYD04_L2" Level 2 (at 10 km spatial resolution at nadir), which combines the Deep Blue (Hsu et al., 2004) and Dark Target (Remer et al., 2005, 2020) MODIS algorithms, to disseminate the AOD global coverage. This merged product provides only high QA pixels. The QA flag in the MODIS product is defined as an integer number, which in the selected combined AOD product is represented by:

- QA > 3 over land and QA > 0 over ocean for the Dark Target
- QA 2 and 3 for the Deep Blue

The MODIS satellite data were resampled at the spatial resolution to match the spatial resolution of the CHIMERE regular grid. For each grid cell, observed AOD was calculated as a weighted average, considering the quality-assurance flags from the MODIS retrievals:

Table 2
Statistical Comparison of the Simulated and Observed Aerosol Optical Depth With Moderate Resolution Imaging Spectroradiometer at 550 nm, Ozone Monitoring Instrument (OMI) at 354 nm, and AERONET Stations at 440 nm

Database	r	NMB (%)
MODIS[a]	0.77	−14
OMI[a]	0.65	−30
AERONET[b,c]	0.79	−23
AERONET-R1[b]	0.78	−35
AERONET-R2[b]	0.77	−20
AERONET-R3[b]	0.76	−16

Abbreviation: AERONET, Aerosol Robotic Network. [a]The comparison is done with monthly average. [b]The comparison is done with daily data. [c]This comparison is done with all AERONET data.

$$\overline{\mathrm{AOD}} = \frac{\sum_i^N \mathrm{AOD}_i \mathrm{QA}_i}{\sum_i^N \mathrm{QA}_i}$$

where $\overline{\mathrm{AOD}}$ is the average AOD in a given pixel. A minimum threshold of 30% of data with a QA score greater than 3 was required for each regridded pixel. The same approach was applied to average the satellite overpass times, extracting the nearest hour to align with the numerical simulation.

The simulated monthly spatial AOD and AAOD patterns at 354 nm were also compared with the OMI Aura Near UV OMAERUV satellite product. Despite the coarse spatial resolution of 13×24 km^2 of the OMI satellite footprint, the OMAERUV algorithm provides aerosol spectral optical properties at 354 and 388 nm (Torres et al., 2007, 2013).

To compare the CHIMERE simulations with OMI data, only QA data (i.e., quality flag = 0) were used, considering pixels with a solar zenith angle <70° and non-missing UV aerosol index values. The OMI satellite data were further resampled to match the spatial resolution of the CHIMERE regular grid. For each grid cell, the AOD/AAOD values were calculated as the average of all satellite pixels falling within the simulation grid.

It should be noted that the comparison of model simulations with observations at specific measurement wavelengths was conducted by interpolating the optical properties simulated by CHIMERE to the wavelengths of the observed AOD and AAOD. This interpolation was achieved using the Ångström exponent and the absorbing Ångström exponent, both calculated from the simulated optical properties. Model accuracy in reproducing observations was assessed using two statistical indices: the Pearson correlation coefficient and the normalized mean bias (NMB). The definition of these indices is provided in Supporting Information S1.

3. Model Evaluation and Results

3.1. Aerosol Optical Depth Simulation

In this section, we assessed the model performance of the reference run (CTRL) in reproducing the AOD, since it is a key indicator of model skill in reproducing aerosol load, which in turn depends on different processes, such as emission, transport, and deposition. This is possible because the AOD changes are negligible between CTRL and improved simulations (Figure S1 in Supporting Information S1). Statistical indices obtained from the model comparison with observed AOD are reported in Table 2.

Figure 4 shows the comparison between monthly average of AOD at 550 nm simulated and observed from the MODIS satellite. CTRL run satisfactorily reproduced the AOD patterns. In particular, the model captured the southeastern aerosol transport, downwind of the Canadian wildfires, toward East Coast of North America and the subsequent outflow on the Atlantic Ocean. The model successfully captured the eastward long-range transport across the ocean and the plume advection over Western Europe. However, the simulated AOD is generally underestimated compared to satellite observations. A more quantitative comparison, as shown in Table 2, indicates that CTRL simulation reproduced the MODIS monthly data with a correlation of 0.77 and average NMB of −14%.

Figure 5 displays the comparison between monthly average AOD at 354 nm simulated by CHIMERE and observed by OMI. CHIMERE captured the AOD distribution retrieved by satellite, especially in Canada close to the boreal fire, Eastern North America, and Atlantic Ocean. The estimated correlation coefficient was 0.65, while the AOD was underpredicted by 30%. A closer inspection to Figure 5 reveals that this bias originates in Western USA, where the model underestimates the observations by a factor of 3–4. This bias may be attributed to the misrepresentation of SOA, which constitutes a significant fraction of aerosol mass in the Western United States (Jimenez et al., 2009) and is likely underestimated in our simulations. This limitation will be further discussed at the end of this Section. In general, the CHIMERE CTRL run performance in reproducing OMI AOD appeared poorer compared to MODIS. The possible reason of this bias will be discussed at the end of this Section.

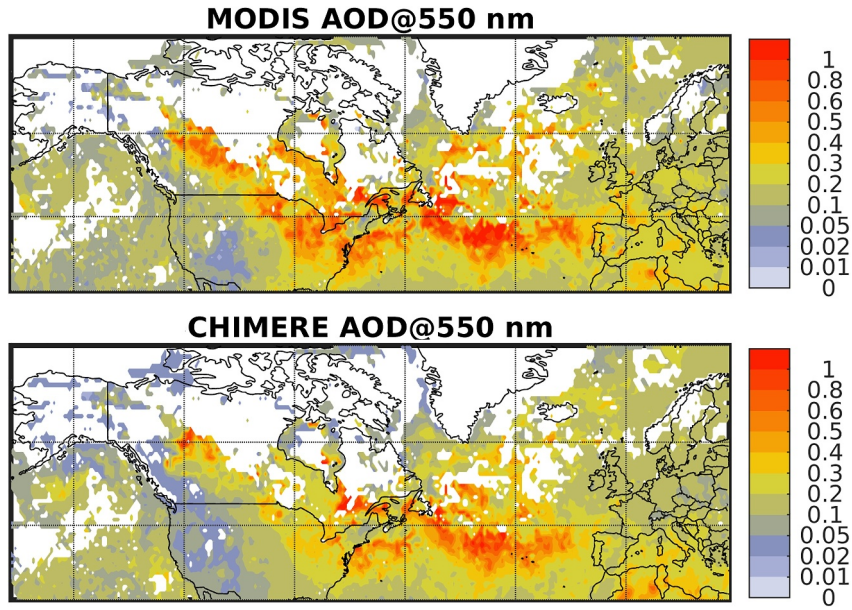

Figure 4. AOD monthly average at 550 nm for June 2023, as measured by Moderate Resolution Imaging Spectroradiometer (upper panel) and modeled by CHIMERE (lower panel).

The comparison of the simulated daily AOD at 440 nm compared with the AERONET at all sites showed a NMB of −24%, while the correlation was 0.79 (see Table 2). Figure 6 depicts the comparison of modeled and observed daily averaged time series of AOD at 440 nm at the R1, R2, and R3 regions. Additionally, the figure also reports the scatter plots between calculated and observed daily AOD values. The model captured the mean daily observed AOD behavior in R1, R2, and R3. The CHIMERE model was able to reproduce the AOD main peaks at the Canadian AERONET sites (R1) in the first half of June, although it did not accurately capture the peaks on June 23 and 25–26. At the same time, the peaks of early, mid, and end June on eastern USA downwind from Canadian sources (R2) were captured, as well as the late June peak on western Europe (R3) due to the long-range smoke transport from North America.

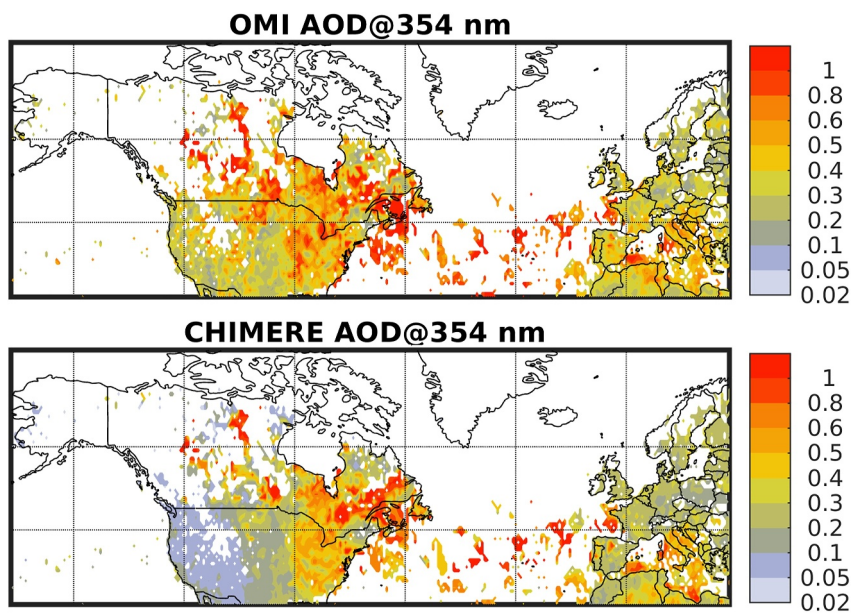

Figure 5. As in Figure 4, but for AOD at 354 nm measured by Ozone Monitoring Instrument (OMI).

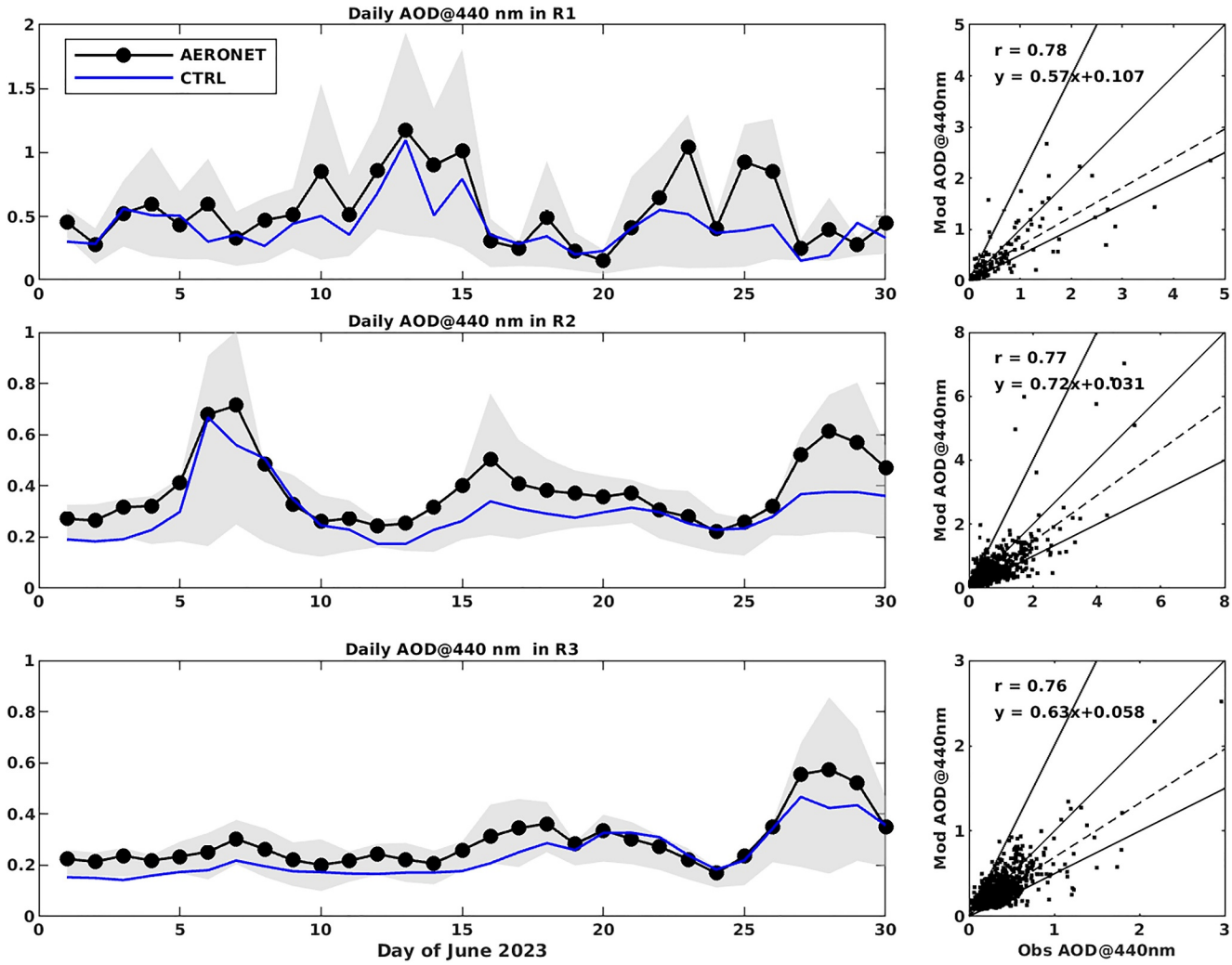

Figure 6. Comparison of AOD at 440 nm simulated by CHIMERE in CTRL run and observed at Aerosol Robotic Network sites. The left panels show the simulated and measured daily time series of AOD, averaged across all stations in regions R1, R2, and R3. The shaded area represents daily 20th and 80th percentile range of observed AOD values for each day. The right panels present the scatter plots of observed versus simulated daily AOD in R1, R2, and R3. The lines 1:1, 2:1, and best least-squares linear fit (dashed lines) are displayed for reference.

Furthermore, the correlation coefficient exceeded 0.70 in all three regions. The NMB was about −20% in R2 and R3, while in R1, it was −35%. The largest bias in R1 could be mainly attributed to the model resolution used in this study that could affect the right position of the wildfire sources. However, it should be noted that even at higher resolution, small errors in simulated wind speed and direction may significantly impact the plume position prediction downwind of the sources (Tuccella et al., 2017). Additionally, the assessment of model performance in R1 may be affected by the limited number (see Figure 3) of AERONET stations available in this region. The potential origins of bias in the simulated AOD magnitude will be discussed at the end of this section.

The same analysis has been conducted for the comparison of modeled AOD at 675 nm with AERONET measurements. Figure S2 in Supporting Information S1 shows the daily averaged times series and daily scatter plots of simulated versus observed AOD at this wavelength. The statistical indices obtained from this comparison are presented in Table S3 in Supporting Information S1. The performance of CHIMERE at this wavelength was similar to that obtained at 440 nm. The correlation coefficient with observed daily values was 0.78, 0.73, and 0.70 in R1, R2, and R3, respectively.

In summary, the outcomes of the statistical analysis obtained from the comparison of the simulated AOD with the AERONET and satellite data are comparable to that of current regional atmospheric models (Curci et al., 2015;

Palacios-Peña et al., 2019). Overall, our model exhibited an underestimation of AOD, which was quantifiable in average between 15% and 30% (see Table 2). This bias has been found in other studies conducted with CHIMERE, even with finer resolutions with respect to the one used in this study (e.g., Menut et al., 2023). Several factors may contribute to a potential bias in the simulated AOD, among those the assumption on particle mixing state (Curci et al., 2015), the simulated aerosol size distribution (Esteve et al., 2014) and the aerosol chemical composition as well as the adopted schemes to represent the inorganic aerosol fraction (Balzarini et al., 2015). For instance, assumptions regarding the aerosol mixing state can influence the AOD by up to 30%–40% (Curci et al., 2015), while uncertainties in the calculation of aerosol size distribution can contribute approximately 35% (Esteve et al., 2014). Additionally, accurate simulation of the chemical composition, particularly the abundance of sulfate and nitrate, is essential for reliably reproducing the AOD (Balzarini et al., 2015). In addition, Konovalov et al. (2023) showed that the parameterization for the secondary organic aerosols used in this study tends to underestimate the SOA mass during wildfire episodes, with consequent bias on the aerosol load. This aspect could be improved by using more realistic SOA schemes available in CHIMERE (such as the Volatility Set Basis scheme), but these are computational expensive for the aim of this investigation, since they would have required many additional variables resulting from the splitting of primary OA sources for BrC simulation. Another important source of bias in this study is the uncertainty of BB emission inventories. Aerosol simulations and their climatic impact are sensitive to specific BB emission inventory (Carter et al., 2020; Y. Liu et al., 2018; Ramnarine et al., 2019). This uncertainty may be larger at high latitudes, where the fire sources in this study are located, due to the increased cloud cover in these regions, which may decrease the accuracy of BB emission estimates (Hua et al., 2024). As noted by Hua et al. (2024), models using current BB emission inventories tend to underestimate AOD at high northern latitudes. Consequently, we speculate that the negative bias in our AOD simulation is likely partially attributable to the BB emission inventory employed.

Additionally, in this discussion, it is essential to consider the uncertainties in the AOD measurements, especially the error associated with satellite data. AERONET has an uncertainty of 0.01–0.02 (Holben et al., 2001), while the error of MODIS is $\pm(0.05 + 0.20 \cdot \mathrm{AOD})$ and $\pm(0.03 + 0.05 \cdot \mathrm{AOD})$ over land and ocean, respectively (Kaufman et al., 1997; Tanré et al., 1997). The average error expected in OMI AOD is of the order of 30% (Torres et al., 2002). We compared AOD retrieved by MODIS and OMI with AERONET data. The comparison of MODIS AOD is shown in Figure S3 in Supporting Information S1. The analysis indicates that MODIS overestimates AOD compared with AERONET, with a monthly average bias of 18%. This positive bias aligns with findings from previous studies. For instance, Gupta et al. (2018) reported an average global bias of +0.03 for MODIS-Aqua data. Specifically, in North America, MODIS AOD tends to be overestimated, particularly over regions with brighter surface backgrounds and areas characterized by steep topographic variations (Jethva et al., 2019). Figure S4 in Supporting Information S1 shows the comparison of OMI AOD with AERONET data, revealing that OMI overestimates AOD by 40%. This bias is particularly evident in the western United States, where we identified the most substantial discrepancies between CHIMERE and OMI data.

3.2. Aerosol Absorption Simulation

In this section, we evaluated the performance of the new absorption scheme implemented within the CHIMERE model and detailed in Sections 2.2 and 2.3. We compared the simulated AAOD for the reference simulation (CTRL), the BC_{Eabs}, and the BEST simulations with the OMI and AERONET AAOD data.

Figure 7 shows the monthly average of AAOD at 354 nm for June 2023, as observed by OMI and simulated by the CHIMERE in the CTRL run, BC_{Eabs}, and BEST simulations. The statistical indices derived from this comparison are reported in Table 3. The spread for these values derived from OMI data error is also reported. OMI AAOD uncertainty is taken as 40%, based on its calculated deviation from AERONET data, as discussed at the end of this section. The correlation coefficient for all the three simulations ranged between 0.50 and 0.54. However, the default model (CTRL), which assumes an external mixing state, failed to reproduce the AAOD observed pattern, exhibiting a bias of −78%. The increase in absorption due to BC_{Eabs} was moderate and primarily localized near the BB sources, where the mass ratio (M_r) reaches its highest values. The overall bias of BC_{Eabs} is reduced by 3% compared to CTRL. A significant improvement in aerosol absorption was observed in BEST simulations. The inclusion of the BrC treatment enabled the model to reproduce the spatial pattern of AAOD much more closely to that observed by OMI. Despite this progress, the mean bias still was −55%. The largest biases in BEST simulations were found in Western USA and North Africa. The latter could be related to the errors in simulating the

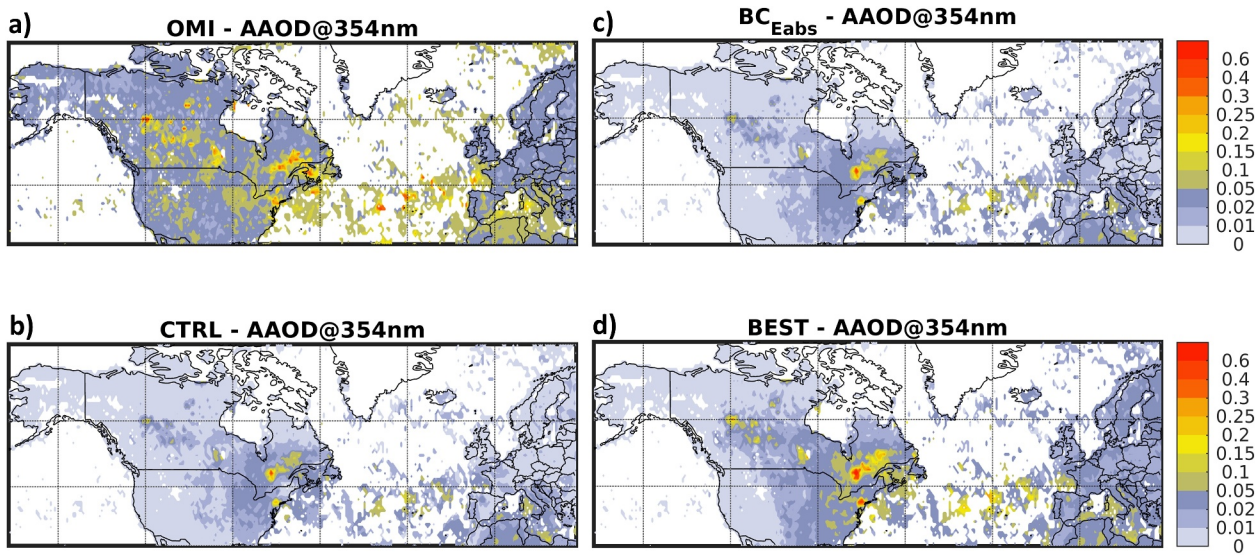

Figure 7. June 2023 monthly average AAOD at 354 nm, (a) as measured by OMI and modeled by CHIMERE in (b) CTRL, (c) BC_{Eabs}, and (d) BEST simulations.

aerosol dust absorption; however, uncertainties in OMI retrievals must also be considered. We will explore this issue in more detail at the end of this section.

Figure 8 shows the comparison of daily AAOD averaged time series at 440 and 675 nm simulated in the CTRL, BC_{Eabs}, and BEST against retrievals from AERONET sites in the R1, R2, and R3 regions. The figure also shows the 20th and 80th percentile range of measurements, along with the error bars associated with the observations. The method used to estimate the uncertainties is described in the Supplements. Generally, the AAOD simulated in CTRL was underestimated, particularly during peak events related to the Canadian forest fires across all three regions. Including the BC absorption enhancement (BC_{Eabs}), a moderate improvement in AAOD simulation was observed at 440 nm. Conversely, at 675 nm, the inclusion of BC E_{abs} resulted in a more accurate simulation of AAOD peaks both near the fire sources (R1) and downwind (R2), as well as in late June over western Europe (R3), attributed to transoceanic smoke transport from North America. This improvement is attributable to the dominance of BC at this wavelength, since BrC primarily absorbs solar radiation in the UV range. Consequently, at 675 nm the BC_{Eabs} and BEST simulations were identical, and the results obtained at this wavelength may be considered an evaluation of BC E_{abs} parameterization.

Figure 9 displays the scatter plots of the daily AAOD at 440 nm simulated in CTRL, BC_{Eabs}, and BEST models with the AAOD measurements from the AERONET sites in R1, R2, and R3. The summary of the statistical indices is reported in Figure 10. In general, the correlation coefficient remained constant across the simulations (about 0.70, 0.64, and 0.53 in R1, R2, and R3, respectively). This indicates that all three of the models were able to capture the temporal variations of absorption. It should be noted that correlation, decreased moving away from the fire sources, most likely because in R1 the AAOD simulation was most affected by BB emissions, while far from boreal wildfires the mixing with other sources may alter the relative contribution of the absorbing and scattering aerosols, lowering the performance indices. When mixing with other air masses occurs, the aerosol composition and mass size distribution might not be accurately represented in the model, leading to potential inaccuracies in M_r and aerosol spectral optical properties. Additionally, the mixing with other sources could influence BrC absorption due to a misrepresentation of photochemical aging processes, which may modify the absorption properties of BrC over time.

Table 3
Statistical Comparison of the Simulated Monthly Absorbing Aerosol Optical Depth at 354 nm in CTRL, BC_{Eabs}, and BEST Simulations With That Observed by OMI

Simulation	r	NMB (%)
CTRL	0.53 (0.48/0.55)	−78 (−81/−49)
BC_{Eabs}	0.54 (0.48/055)	−75 (−78/−42)
BEST	0.50 (0.42/50)	−55 (−60/+6)

The CTRL simulation underpredicted the AAOD by 18% in R1, while it became negligible after including BC enhancement in the model. The addition of the BrC absorption (BEST), lead to a positive bias of +30%. This result could be attributed to the presence of "browner" BB-BrC, whose absorption could be overestimated, given its highly uncertain MAC. Moreover,

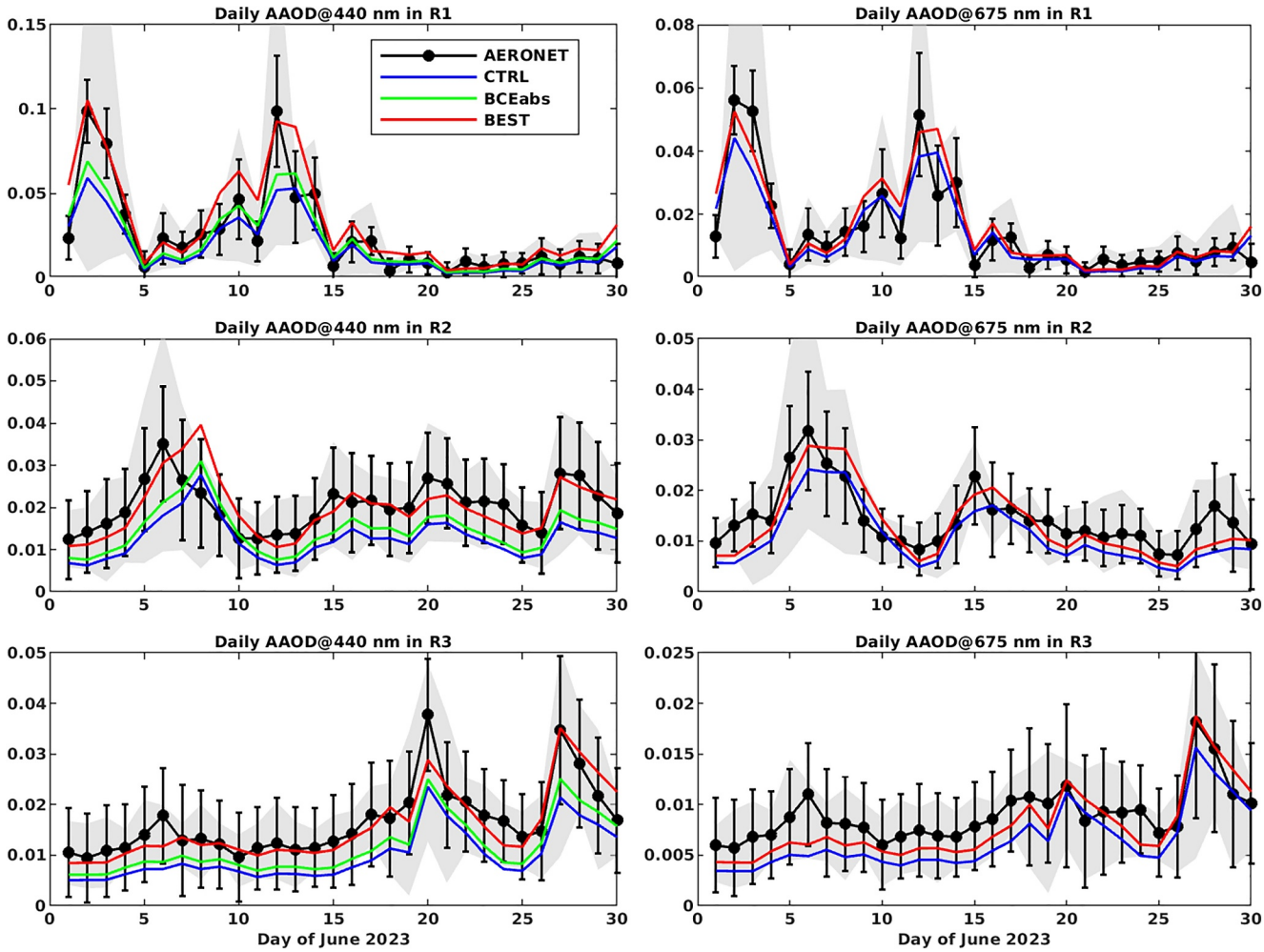

Figure 8. Comparison observed and modeled average time series of AAOD at 440 (left panels) and 675 nm (right panels), for the CTRL (blue), BC_{Eabs} (green), and BEST (red) simulations at Aerosol Robotic Network sites in regions R1, R2, and R3. Shaded areas denote the 20th to 80th percentile range of observed AAOD values for each day, while vertical bars represent the observational uncertainties. Please, note that at 675 nm BC_{Eabs}, and BEST give the same results, since brown carbon has limited absorbing at this wavelength.

as highlighted also in Section 3.1 for the AOD, model evaluation in R1 may be affected by the limited number of AERONET observations available in this area. The bias in the CTRL simulation was −40% for both R2 and R3. In contrast, the BC_{Eabs} simulation showed a bias of −25% in both these regions, whilst BEST run exhibited a slight positive bias in both R2 and R3.

The same analysis has been performed for AAOD at 675 nm. The results of the comparison are reported in Figures S4 and S5 in Supporting Information S1. As for AAOD at 440 nm, the correlation coefficient was constant across model simulations and decreased moving away from boreal wildfires. Its values were about 0.75, 0.65, and 0.45 in R1, R2, and R3 respectively. In R1, NMB was negligible in CTRL, but it increased at +25% in BC_{Eabs}. CTRL underestimated the AAOD at 675 nm by 18% and 26% in R2 and R3, respectively. Adding the BC absorption enhancement, the bias became negligible in R2 and reduced to −9% in R3.

In summary, the evaluation demonstrated that the new absorption scheme implemented in CHIMERE overall enhances the model skill in reproducing the observed AAOD patterns. The uncertainties of absorption treatment used in this work are mostly related to the missing of some blanching effects due to in-cloud processes of primary BrC and SOA aging. Additionally, assumptions regarding the MAC of browner BB-BrC could introduce further uncertainty. Furthermore, the uncertainties could also arise from the simplified parameterization of E_{abs}. In our model, the absorption enhancement predicted by core-shell model ($E_{abs_{cs}}$) is maintained at the fixed value of 1.5,

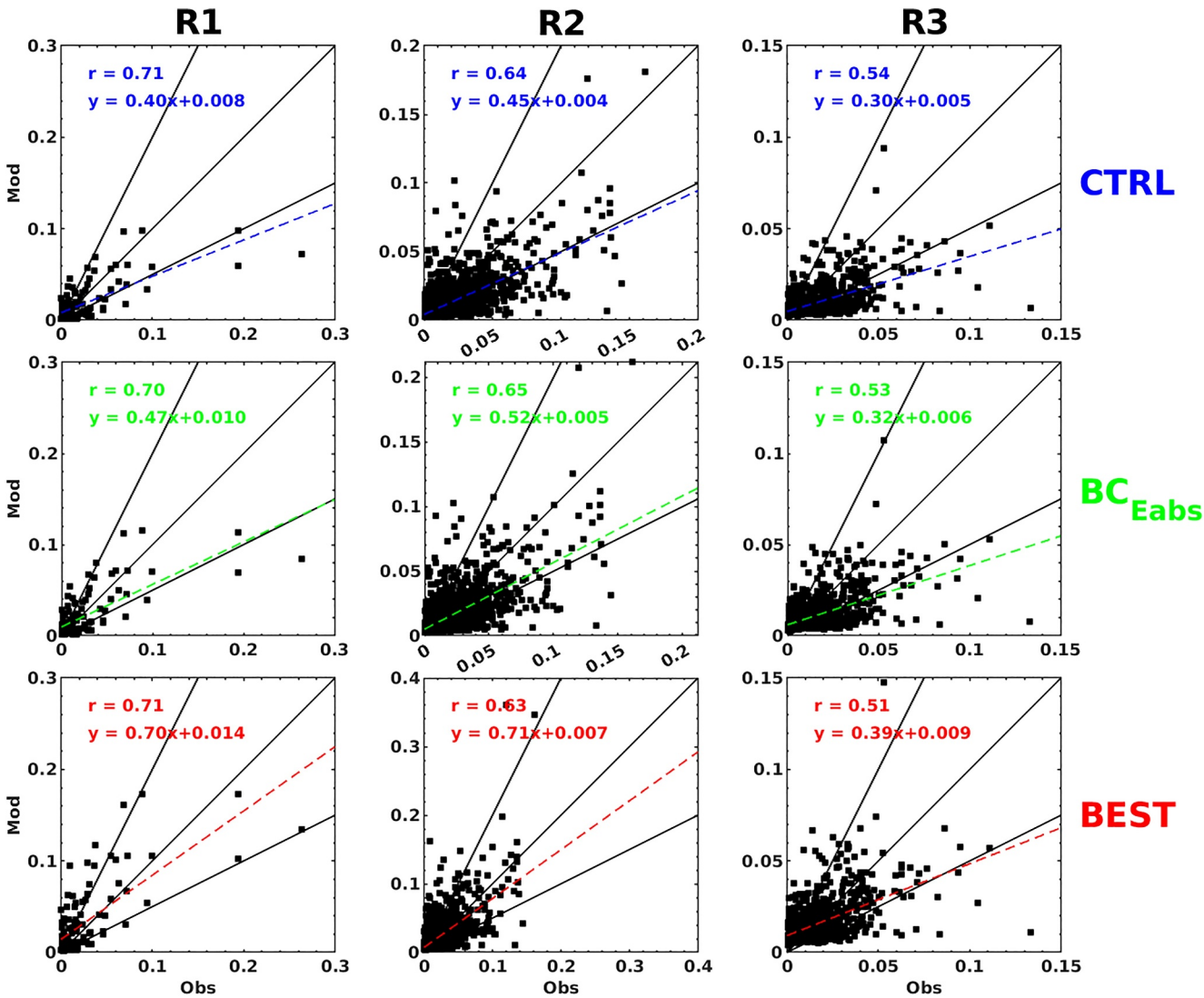

Figure 9. Scatter plots of observed and modeled daily AAOD at 440 nm, for the CTRL, BC_{Eabs}, and BEST simulations at Aerosol Robotic Network sites in regions R1, R2, and R3. The lines 1:1, 2:1, and best least-squares linear fit (dashed lines) are displayed for reference.

which may not accurately capture the variability observed under different atmospheric conditions. A more detailed discussion of these aspects may be found in Section 5.

Moreover, uncertainties associated with AERONET and OMI data could affect the model comparison with observations. In our analysis, we complemented the L2.0 of AERONET for AAOD with L1.5 measurements, as AAOD in the L2 data set was provided only for AOD at 440 nm larger than 0.4. The uncertainty of SSA, used to derive AAOD, is site dependent. Generally, the uncertainty related to SSA retrieval varies with AOD, ranging from approximately ±0.03 for AOD at 440 nm greater than 0.5 to ±0.05–0.07 for AOD less than 0.2 (Sinyuk et al., 2020). Furthermore, this uncertainty increases with larger wavelengths. Concerning the uncertainty of OMI retrieval, the comparison of OMI AAOD with AERONET data is displayed in Figure S5 in Supporting Information S1. OMI shows an average positive bias of 66% with respect to AERONET. The most considerable discrepancies between AERONET and OMI data are found in the western United States, where we noted the most important error in CHIMERE AAOD simulation with respect to OMI data. There are several factors contributing to OMI AAOD bias. First, as noted by Schutgens et al. (2021), the agreement between satellite-derived AAOD and SSA and AERONET data improves with increasing AOD. As shown in Figure 2b, Western United States is the region that exhibits the lowest average AOD values. Consequently, we may expect a higher uncertainty in OMI retrievals in this area. Additional sources of uncertainty in OMI AAOD include subpixel cloud

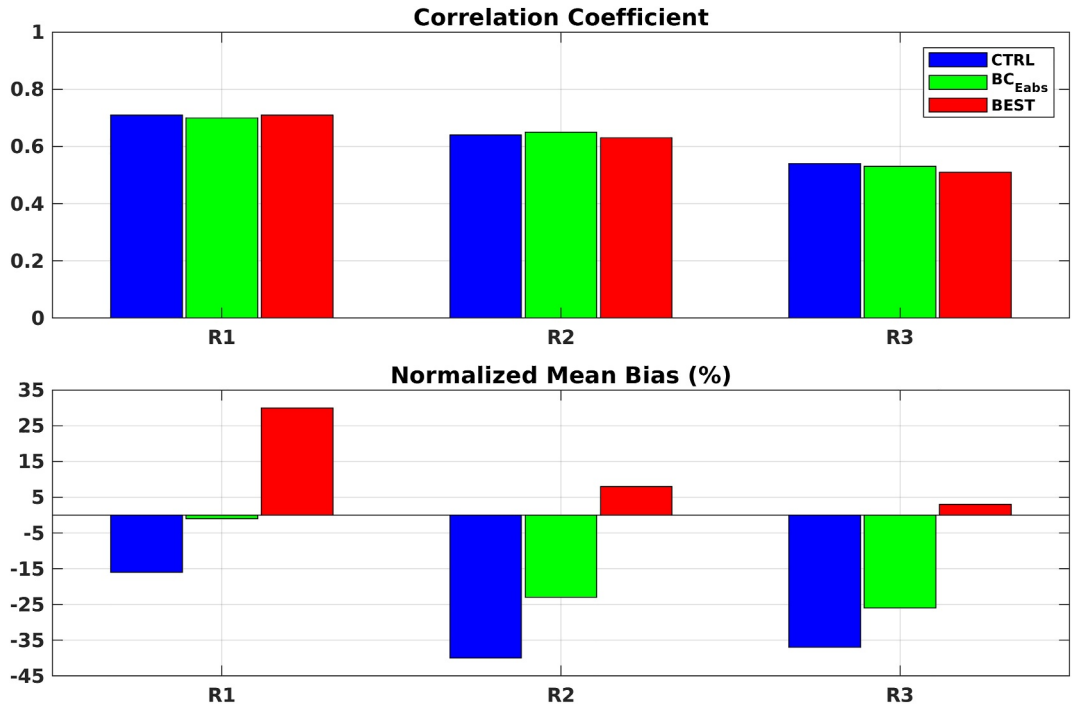

Figure 10. Statistical summary of the comparison of observed and modeled daily AAOD at 440 nm, for the CTRL, BC_{Eabs}, and BEST simulations, at Aerosol Robotic Network sites in regions R1, R2, and R3.

contamination within the satellite footprint (13 × 24 km for nadir pixels), assumptions about aerosol layer height, aerosol microphysical and optical properties, and the accuracy of the prescribed surface albedo (Jethva & Torres, 2019).

3.3. Direct Radiative Effect

In this section, we have assessed the impact of new treatment of BC and OA absorption on the AAOD simulation and its implication for the DRE. This analysis was conducted over the regular CHIMERE domain.

Figure 11 shows the total and BB aerosols average AAOD at 550 nm for June 2023, as calculated in CTRL and BEST simulations. The domain averages of AAOD are reported in Table 4. The total average AAOD was 0.0068 in CTRL simulation, while in the enhanced model (BEST) it increased to 0.0089 (+31%). In the Canadian wildfire source regions, AAOD in the BEST simulation increased by 35%–40% relative to the CTRL run, with some areas showing a rise of up to 45% (Figure S6 in Supporting Information S1). The relative increase in AAOD could reach up to 50% in regions where BB aerosols are mixed with BF sources, such as in the southeastern USA. Over the Atlantic Ocean and the Arctic, the relative increase was 30%–35%. A 35%–40% increase was also observed over Eastern Europe, largely due to BF emissions of OA. AAOD due to BB was 0.0047 in the CTRL run and increased to 0.0066 (+40%) in BEST simulation. According to our model, BB contributes approximately 74% to the total aerosol absorption within the considered domain. The sensitivity of domain-average AAOD from the enhanced model was evaluated by comparing the BEST run with extreme absorption scenarios (L-ABS and H-ABS tests), resulting in a sensitivity range of −10/+24% for total AAOD and −14/+30% for BB AAOD.

DRE at the top of the atmosphereltop of the atmosphere (TOA) has been calculated offline with a simplified formalization provided by Seinfeld and Pandis (2016). The details of this formulation are reported in Section S2 in Supporting Information S1 of the Supplementary Material. DRE has been calculated only for shortwave radiation, since the impact of BC and OA on longwave radiation is negligible (see, for instance, Table 3 in Heald et al., 2014).

Figure 12 displays the average BB all-sky DRE for June 2023, as calculated in CTRL and BEST simulations. Table 5 reports the domain averages of all-sky TOA DRE. For completeness, the clear-sky TOA DRE is also

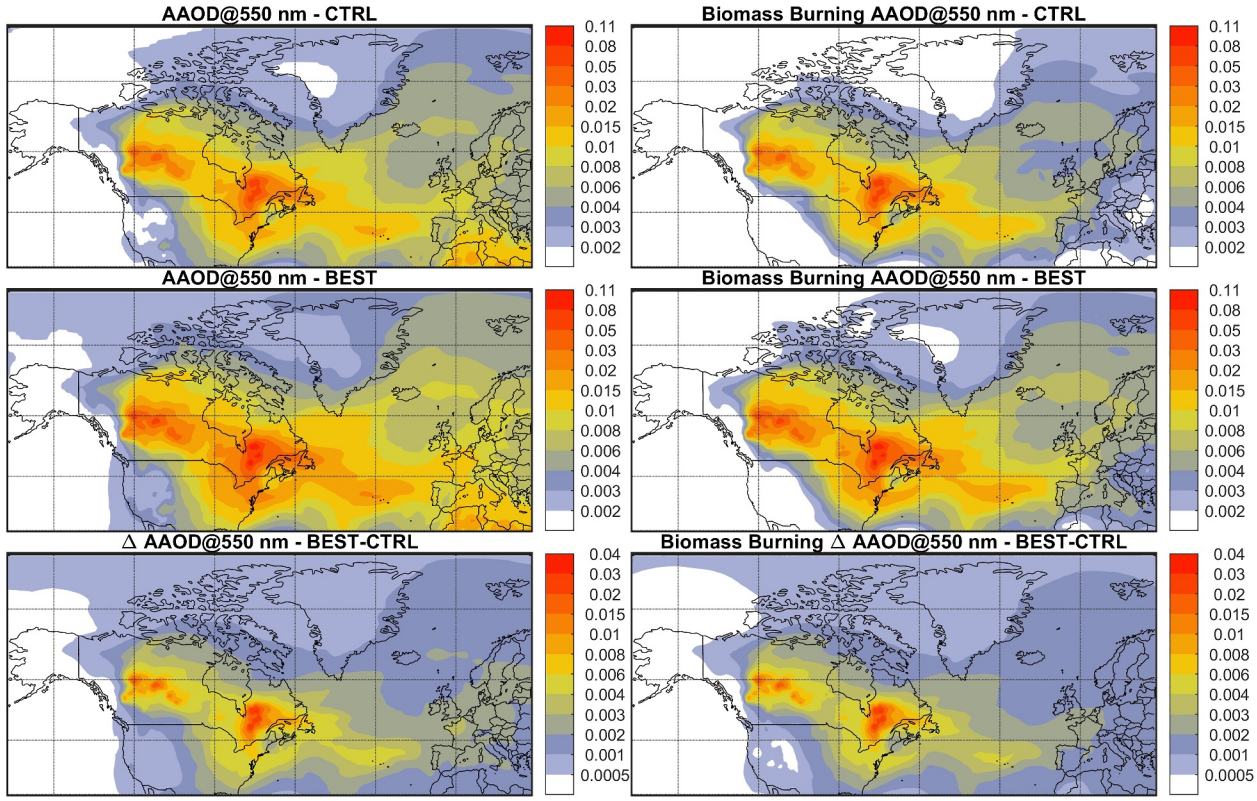

Figure 11. Mean total (left panels) and biomass burning (right panels) AAOD at 550 for June 2023, calculated by the CTRL (upper panels) and BEST (middle panels) models, and their difference (lower panels).

reported. The sensitivity associated with the DRE from the enhanced model was evaluated using the same approach as for AAOD.

In the default model, the all-sky DRE related to the intense Canadian wildfire event was −2.1 W/m^2, with the strongest cooling effects observed over oceans and land, reaching −30/−20 W/m^2 near the BB sources in Canada. By contrast, warming effects were observed over snow-covered land and sea ice, with a warming of up to 10–15 W/m^2 in Arctic regions downwind of the BB sources.

In the BEST model, the all-sky DRE was reduced to −1.9 W/m^2 (−2.0/−1.8 W/m^2, ±5%), indicating an additional monthly average warming of +0.2 W/m^2 (+10%) in the enhanced model simulation of the Canadian wildfire climatic impact. This supplemental warming was most pronounced over snow/ice-covered regions, with a DRE reduction up to 2.5–3.0 W/m^2 in North America downwind of the fires and up to 2.0–2.5 W/m^2 in southern Greenland. The cooling effect in BEST was also reduced by up to 1.5 W/m^2 in Canada near the source regions and by few tens of W/m^2 over the Atlantic Ocean and Europe.

Table 4
Total Aerosol and Biomass Burning (BB) Average AAOD at 550 nm for June 2023, Calculated CTRL and BEST Simulations

	CTRL	BEST	Sensitivity RANGE[a]
AAOD	0.0068	0.0089	0.0080/0.0110 (−10/+24%)
BB-AAOD	0.0047	0.0066	0.0057/0.0086 (−14/+30%)

[a]The sensitivity range has been assessed relative to BEST simulation, using L-ABS and H-ABS sensitivity tests.

Finally, it is insightful to examine the variation in DRE between the default and enhanced models, normalized to the change in AAOD at 550 nm between the two simulations. The resulting normalized BB all-sky ΔDRE was 1.05 W/m^2/AAOD × 10^{-2}. This value suggests a significant DRE sensitivity to AAOD change in the model.

These results emphasize that accurate calculation of BC and BrC sunlight absorption is crucial for understanding the impact of intense boreal wildfires on regional climate. Our findings suggest that models lacking proper treatment of carbonaceous aerosol absorption may overestimate the cooling effect of boreal wildfires. Therefore, improving aerosol absorption parameterizations is crucial, along with incorporating the feedback between climate and

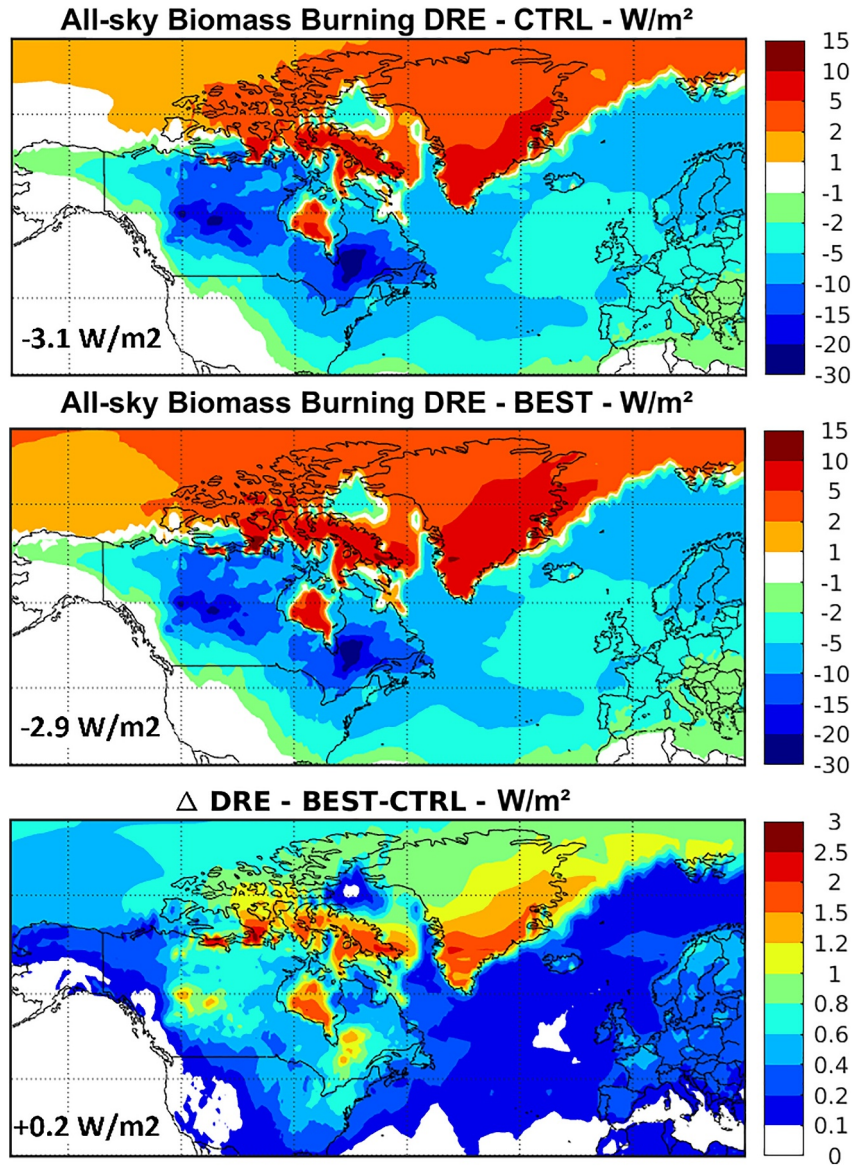

Figure 12. Mean all-sky direct radiative effect of BB aerosols at the top of the atmosphere|top of the atmosphere for June 2023, calculated by the CTRL (upper panel) and BEST (middle panel) models, and their difference (lower panel).

aerosol smoke from boreal fires, both in near-future climate simulations and the development of effective mitigation strategies. Recent study of Allen et al. (2024) suggest that anthropogenic aerosol mitigation strategies will likely increase boreal forest fires, but the full impact of resulting emissions on the climate system remains uncertain. Without adequate treatment of BC and BrC absorption, the climatic effect of these emissions could be significantly misrepresented.

4. Discussion of the Limitations

In this Section, we have discussed the limitations and uncertainties that affected our results.

A primary source of uncertainty in our study is linked to the model setup, specifically to the scheme adopted for simulating SOA, which may affect $E_{abs.}$ This scheme is based on the single-step oxidation, which tends to underestimate SOA concentrations. Consequently, the fraction of internally mixed BC might also be lower than expected, as the BC mass ratio (M_r) is likely underpredicted due to errors in SOA representation. This, in turn, is

Table 5
June 2023 Average Clear-Sky and All-Sky TOA Direct Radiative Effect (W/m2) of Biomass Burning (BB) Calculated From CTRL and BEST Simulations

	CTRL	BEST	Sensitivity range[a]
Clear-sky	−3.1	−2.8	−3.0/−2.6 (−7/+7%)
All-sky	−2.1	−1.9	−2.0/−1.8 (−5/+5%)

[a]The sensitivity range has been assessed relative to BEST simulation, using L-ABS and H-ABS sensitivity tests.

likely contributing to an underestimation of BC absorption. Another potential limitation linked to the simulation setup could be related to the use of 2022 anthropogenic emissions for simulating the 2023 aerosol concentration, in particular in regions where BF aerosols may contribute significantly to absorption. However, given that BB emissions largely dominated BrC and BC absorption during June 2023 and that year-to-year variations in anthropogenic emissions are generally small, unless driven by major changes in human activities, such as those observed during the COVID-19 pandemic or in response to large-scale emission reduction policies, the impact of using 2022 anthropogenic emissions is expected to be negligible.

A second limitation of our work is about the BC absorption treatment. In our model, we have assumed $E_{abs_{cs}}$ as a constant value. Actually, this value may depend on various factors, such as the chemical composition, amount of the coating material, and coating thickness. For instance, Zhang et al. (2018) demonstrated that under typical conditions observed in their study conducted in the Paris area, E_{abs} was sensitive to an increase in the SOA mixing ratio, while it remained unchanged with increasing sulfate concentration. On the other hand, Yus-Díez et al. (2022) found that in two Mediterranean sites, E_{abs} exponentially increases with the amount of material available for coating. Shiraiwa et al. (2010) further showed that BC absorption increases with coating thickness. Specifically, absorption increased by 30% when the shell-to-core diameter ratio was 1.2 and doubles when the ratio reached 2. Consequently, the assumption of a constant $E_{abs\ CS}$ may oversimplify the complex interactions that govern BC absorption enhancement. This could lead to under- or overestimation of BC E_{abs}, particularly in regions where the chemical composition or physical properties of the aerosol population deviate from the average conditions underlying the assumed constant $E_{abs\ CS}$ value of 1.5.

The presence of BrC in the shell is another critical factor missed in our model that deserves attention. In general, the assumed average value of $E_{abs\ CS}$ may already account for BrC absorption. Consequently, this could lead to an overestimation of absorption, as BrC absorption might be effectively double-counted, first as part of the shell and again as externally mixed BrC (Wang et al., 2018). At the same time, it is important to note that the assumed average $E_{abs\ CS}$ of 1.5 in our model may actually underestimate absorption when BrC is included in the coating material. In such cases, E_{abs} may fall within in the range of 2–5 (Cheng et al., 2017; Luo et al., 2018). In our previous work, we found that the global average value of E_{abs} at AERONET sites from multiyear simulations was 3.4 when BrC was included in the shell (Tuccella et al., 2020).

The approach for implementing the BrC in CHIMERE presents some limitations. These are related to aging processes that were missed in our implementation. First, our model does not account for the blanching effect due to in-cloud water processing, which should reduce the browner BrC lifetime of about 3 hr (Hems et al., 2021). Second, we have not included in the model the blanching that SOA-BrC could undergo with aging (Kasthurirachchi et al., 2020; Lee et al., 2014; J. Liu et al., 2016). The omission of these aging processes is likely to result in an overestimation of BrC AAOD and its DRE. Additionally, the MAC for browner BB-BrC was set at 150% higher than that of freshly emitted. It is important to note that this value falls within the middle range of those observed in laboratory studies (Hems et al., 2021; Zhong and Jang, 2014). As a result, this assumption may influence BrC absorption near BB sources, where browner BrC is more prevalent. Indeed, we observed an overestimation of the AAOD in regions close to BB sources, which is likely attributable to this assumption.

Finally, we have assigned to all the SOA-BrC derived compounds the same imaginary part of the complex refractive index. However, the absorption of secondary BrC could be dependent on the specific SOA precursor and oxidation patterns. For example, the absorption of SOAs formed from photochemical oxidation of toluene appears to strongly depend on the initial NO_x concentration (Dingle et al., 2019; Lin et al., 2015; P. F. Liu et al., 2015; Moise et al., 2025). This assumption is likely to reduce the regional variability of the BrC-SOA absorption.

5. Conclusions

BC and BrC are light-absorbing aerosols which play a key role in the climatic system. Boreal wildfires are significant sources of these particles. Boreal wildfire events are increasing due to climate change. Accurate modeling of BC and BrC absorption is essential for simulating the DRE of these events. In this study, we modeled

the BC and BrC absorption during the severe Canadian wildfires of June 2023 using an enhanced CHIMERE model and assessed the impact of these improvements on the DRE of the wildfires.

The CHIMERE model was configured on a large domain spanning from North America to Eastern Europe, including the high latitude up to 75°N. We implemented in the model a parameterization for BC absorption enhancement (E_{abs}), which depends on the mixing state of BC particles, through the mass ratio of non-BC to BC aerosols, according to the work of Liu et al. (2017). We also implemented an advanced scheme for BrC absorption, which accounts for "browning" and "blanching" processes due to photochemical aging, following the approach of DeLessio et al. (2024). A series of simulations were conducted to assess the impact of BC E_{abs} and BrC on aerosol absorption simulation. Model performance was evaluated through a statistical comparison with AOD and AAOD data from satellite instruments (MODIS and OMI) and ground-based AERONET stations, focusing on regions impacted by Canadian wildfires.

The model captured the spatial patterns of AOD, particularly the long-range transport of aerosols from Canadian wildfires toward the East Coast of North America and across the Atlantic to Europe. The model generally underestimated AOD compared with satellite observations, with biases ranging from 15% to 30%. Correlation coefficients for the comparison with MODIS and OMI AOD were 0.77 and 0.65, respectively, while comparisons with AERONET showed a correlation of 0.79 and a bias of −24%.

The default model (CTRL) underestimated AAOD retrieved by OMI, particularly near BB sources, with a bias of up to −78%. A moderate improvement was observed by including in model the BC absorption enhancement (BC_{Eabs}), but the most substantial advancements were achieved in the BEST simulations, which included both E_{abs} and BrC treatment, improving spatial patterns and statistical indices. The model comparison with AAOD measurements at 440 and 675 nm from AERONET exhibited a correlation of about 0.75 near the wildfire sources, which tends to decrease moving downwind from these sources. In general, the CTRL run underestimated the observed AAOD, while a significant improvement of the model was obtained in the BEST simulation.

The enhanced model (BEST) increased the monthly domain average AAOD at 550 nm by 31% compared with the CTRL, with the most significant changes observed near the Canadian wildfires and areas where BB aerosols mixed with fossil fuel sources. Canadian smoke aerosols contributed approximately to 74% of total aerosol absorption.

The all-sky TOA DRE associated with the Canadian wildfires of June 2023 was estimated to be −2.1 W/m^2 in the CTRL run. In the best simulation, this value was reduced to −1.9 W/m^2, indicating an additional warming of +0.2 W/m^2 (+10%), attributable to the enhanced treatment of BC and BrC absorption. The increased in DRE calculated in BEST was more pronounced in the regions covered by snow and ice, such as the Arctic and Southern Greenland. Furthermore, the normalized all-sky DRE change resulting from the increase in AAOD obtained in BEST simulation was +105 W/m^2/AAOD, highlighting the critical role of aerosol absorption in radiative balance during the intense boreal wildfire events.

The results of this study could be improved by employing a more advanced scheme for the SOA formation, such as the volatile basis set scheme, which accounts for the OA volatility. Furthermore, the simulation of BC absorption could be refined by adopting an explicit model for core-shell structures, incorporating BrC absorption in the shell, rather than using a constant E_{abs}. Lastly, the accuracy of absorption calculations could be improved by including a representation of BrC blanching due to in-cloud processes within the model. However, to evaluate the model sensitivity to absorption properties, we perturbed the BEST simulation with low and high absorption scenarios. The results indicate a sensitivity range of −14%/+30% in BB-AAOD and −5/+5% in the all-sky DRE estimate attributed to Canadian wildfires.

Overall, the findings of this investigation demonstrate the importance of an accurate simulation of BC and BrC absorption to properly assess the regional climatic impact of intense boreal wildfire. The lack of this factor in the models may results in an overestimation of the radiative cooling effect of boreal fires. Consequently, improving the parameterizations of carbonaceous aerosol absorption is essential for reliable near-future climatic predictions and for evaluating the impacts of the aerosol mitigation strategies.

Conflict of Interest

The authors declare no conflicts of interest relevant to this study.

Data Availability Statement

[Dataset] CHIMERE simulations are available at Tuccella (2024). AERONET data are freely available at the following website https://aeronet.gsfc.nasa.gov/new_web/data.html. MODIS and OMI data may be downloaded at https://disc.gsfc.nasa.gov/. [Software] Model code is available at Tuccella (2024).

Acknowledgments
The authors are grateful to three anonymous reviewers for their suggestions and constructive comments that helped to improve this paper. We thank also NASA for making freely available the MODIS, OMI, and AERONET measurements. This work was not supported by any external funding. Open access publishing facilitated by Università degli Studi dell'Aquila, as part of the Wiley - CRUI-CARE agreement.

References

Adachi, K., Chung, S. H., & Buseck, P. R. (2010). Shapes of soot aerosol particles and implications for their effects on climate. *Journal of Geophysical Research*, *115*(D15), D15206. https://doi.org/10.1029/2009JD012868

Alexander, D. T. L., Crozier, P. A., & Anderson, J. R. (2008). Brown carbon spheres in East Asian outflow and their optical properties. *Journal of Geophysical Research*, *321*(5890), 833–836. https://doi.org/10.1126/science.1155296

Alfaro, S. C., & Gomes, L. (2001). Modeling mineral aerosol production by wind erosion: Emission intensities and aerosol size distribution in source areas. *Journal of Geophysical Research*, *106*(D16), 18075–18084. https://doi.org/10.1029/2000JD900339

Allen, R. J., Samset, B. H., Wilcox, L. J., & Fisher, R. A. (2024). Are Northern Hemisphere boreal forest fires more sensitive to future aerosol mitigation than to greenhouse gas–driven warming? *Science Advances*, *10*(13), eadl4007. https://doi.org/10.1126/sciadv.adl4007

Andreae, M. O., & Gelencsér, A. (2006). Black carbon or brown carbon? The nature of light-absorbing carbonaceous aerosols. *Atmospheric Chemistry and Physics*, *6*(10), 3131–3148. https://doi.org/10.5194/acp-6-3131-2006

Arola, A., Stu, G., Kazadzis, S., Dey, S., & Tripathi, S. N. (2011). Inferring absorbing organic carbon content from AERONET data. *Atmospheric Chemistry and Physics*, *11*(1), 215–225. https://doi.org/10.5194/acp-11-215-2011

Balzarini, A., Pirovano, G., Honzak, L., Žabkar, R., Curci, G., Forkel, R., et al. (2015). WRF-Chem model sensitivity to chemical mechanisms choice in reconstructing aerosol optical properties. *Atmospheric Environment*, *115*, 604–619. https://doi.org/10.1016/j.atmosenv.2014.12.033

Bessagnet, B., Menut, L., Curci, G., Hodzic, A., Guillaume, C., Liousse, C., et al. (2008). Regional modeling of carbonaceous aerosols over Europe-Focus on secondary organic aerosols. *Journal of Atmospheric Chemistry*, *61*(3), 175–202. https://doi.org/10.1007/s10874-009-9129-2

Bond, T. C., & Bergstrom, R. W. (2006). Light absorption by carbonaceous particles: An investigative review. *Aerosol Science & Technology*, *40*(1), 27–67. https://doi.org/10.1080/02786820500421521

Bond, T. C., Bhardwaj, E., Dong, R., Jogani, R., Jung, S. K., Roden, C., et al. (2007). Historical emissions of black and organic carbon aerosol from energy-related combustion. *Global Biogeochem*, *21*(2), 1850–2000. https://doi.org/10.1029/2006GB002840

Bond, T. C., Doherty, S. J., Fahey, D. W., Forster, P. M., Berntsen, T., De Angelo, B. J., et al. (2013). Bounding the role of black carbon in the climate system: A scientific assessment. *J. Geophys. Res.-Atmos.*, *118*(11), 5380–5552. https://doi.org/10.1002/jgrd.50171

Bondy, A., Bonanno, D., Moffet, R., Wang, B., Laskin, A., & Ault, A. (2018). The diverse chemical mixing state of aerosol 430 particles in the southeastern United States. *Atmospheric Chemistry and Physics*, *18*(16), 12595–12612. https://doi.org/10.5194/acp-18-12595-2018

Bones, D. L., Henricksen, D. K., Mang, S. A., Gonsior, M., Bateman, A. P., Nguyen, T. B., et al. (2010). Appearance of strong absorbers and fluorophores in limonene-O3 secondary organic aerosol due to NH4+ mediated chemical aging over long time scales. *Journal of Geophysical Research*, *115*(D5), D05203. https://doi.org/10.1029/2009JD012864

Briant, R., Tuccella, P., Deroubaix, A., Khvorostyanov, D., Menut, L., Mailler, S., & Turquety, S. (2017). Aerosol–radiation interaction modelling using online coupling between the WRF 3.7.1 meteorological model and the CHIMERE 2016 chemistry-transport model, through the OASIS3-MCT coupler. *Geoscientific Model Development*, *10*(2), 927–944. https://doi.org/10.5194/gmd-10-927-2017

Brown, H., Liu, X., Feng, Y., Jiang, Y., Wu, M., Lu, Z., et al. (2018). Radiative effect and climate impacts of brown carbon with the Community Atmosphere Model (CAM5). *Atmospheric Chemistry and Physics*, *18*(24), 17745–17768. https://doi.org/10.5194/acp-18-17745-2018

Brown, H., Liu, X., Pokhrel, R., Murphy, S., Lu, Z., Saleh, R., et al. (2021). Biomass burning aerosols in most climate models are too absorbing. *Nature Communications*, *12*(1). 277. https://doi.org/10.1038/s41467-020-20482-9

Brown, H., Wang, H., Flanner, M., Liu, X., Singh, B., Zhang, R., et al. (2022). Brown carbon fuel and emission source attributions to global snow darkening effect. *Journal of Advances in Modeling Earth Systems*, *14*(4), e2021MS002768. https://doi.org/10.1029/2021MS002768

Byrne, B., Liu, J., Bowman, K. W., Pascolini-Campbell, M., Chatterjee, A., Pandey, S., et al. (2024). Carbon emissions from the 2023 Canadian wildfires. *Nature*, *633*(8031), 835–839. https://doi.org/10.1038/s41586-024-07878-z

Cappa, C. D., Onasch, T. B., Massoli, P., Worsnop, D. R., Bates, T. S., Cross, E. S., et al. (2012). Radiative absorption enhancements due to the mixing state of atmospheric black carbon. *Science*, *337*(6098), 1078–1081. https://doi.org/10.1126/science.1223447

Carter, T. S., Heald, C. L., Jimenez, J. L., Campuzano-Jost, P., Kondo, Y., Moteki, N., et al. (2020). How emissions uncertainty influences the distribution and radiative impacts of smoke from fires in North America. *Atmospheric Chemistry and Physics*, *20*(4), 2073–2097. https://doi.org/10.5194/acp-20-2073-2020

Chen, F., & Dudhia, J. (2001). Coupling an advanced land surface-hydrology model with the penn state-NCAR MM5, modeling system. Part I: Model implementation and sensitivity. *Monthly Weather Review*, *129*(4), 569–585. https://doi.org/10.1175/1520-0493(2001)129<0569:CAALSH>2.0.CO;2

Chen, Y., & Bond, T. C. (2010). Light absorption by organic carbon from wood combustion. *Atmospheric Chemistry and Physics*, *10*(4), 1773–1787. https://doi.org/10.5194/acp-10-1773-2010

Cheng, Y., He, K. B., Engling, G., Weber, R., Liu, J. M., Du, Z. Y., & Dong, S. P. (2017). Brown and black carbon in Beijing aerosol: Implications for the effects of brown coating on light absorption by black carbon. *Science of the Total Environment*, *599*, 1047–1055. https://doi.org/10.1016/j.scitotenv.2017.05.061

Cheng, Z., Atwi, K. M., Yu, Z., Avery, A., Fortner, E. C., Williams, L., et al. (2020). Evolution of the light-absorption properties of combustion brown carbon aerosols following reaction with nitrate radicals. *Aerosol Science & Technology*, *54*(7), 849–863. https://doi.org/10.1080/02786826.2020.1726867

Craig, A., Valcke, S., & Coquart, L. (2017). Development and performance of a new version of the OASIS coupler, OASIS3-MCT_3.0. *Geoscientific Model Development*, *10*(9), 3297–3308. https://doi.org/10.5194/gmd-10-3297-2017

Curci, G., Alyuz, U., Barò, R., Bianconi, R., Bieser, J., Christensen, J. H., et al. (2019). Modelling black carbon absorption of solar radiation: Combining external and internal mixing assumptions. *Atmospheric Chemistry and Physics*, *19*(1), 181–204. https://doi.org/10.5194/acp-19-181-2019

Curci, G., Hogrefe, C., Bianconi, R., Im, U., Balzarini, A., Baro, R., et al. (2015). Uncertainties of simulated aerosol optical properties induced by assumptions on aerosol physical and chemical properties: An AQMEII-2 perspective. *Atmospheric Environment*, *115*, 541–552. https://doi.org/10.1016/j.atmosenv.2014.09.009

DeLessio, M. A., Tsigaridis, K., Bauer, S. E., Chowdhary, J., & Schuster, G. L. (2024). Modeling atmospheric brown carbon in the GISS ModelE Earth system model. *Atmospheric Chemistry and Physics*, *24*(10), 6275–6304. https://doi.org/10.5194/acp-24-6275-2024

Derognat, C., Beekmann, M., Baeumle, M., Martin, D., & Schmidt, H. (2003). Effect of biogenic volatile organic compound emissions on tropospheric chemistry during the Atmospheric Pollution over the Paris Area (ESQUIF) campaign in the Ile-de-France region. *Journal of Geophysical Research*, *108*(D17), 8560. https://doi.org/10.1029/2001JD001421

Dingle, J. H., Zimmerman, S., Frie, A. L., Min, J., Jung, H., & Bahreini, R. (2019). Complex refractive index, single scattering albedo, and mass absorption coefficient of secondary organic aerosols generated from oxidation of biogenic and anthropogenic precursors. *Aerosol Science & Technology*, *53*(4), 449–463. https://doi.org/10.1080/02786826.2019.1571680

Drugé, T., Nabat, P., Mallet, M., Michou, M., Rémy, S., & Dubovik, O. (2022). Modeling radiative and climatic effects of brown carbon aerosols with the ARPEGE-Climat global climate model. *Atmospheric Chemistry and Physics*, *22*(18), 12167–12205. https://doi.org/10.5194/acp-22-12167-2022

Dubovik, O., Holben, B., Eck, T. F., Smirnov, A., Kaufman, Y. J., King, M. D., et al. (2002). Variability of absorption and optical properties of key aerosol types observed in worldwide locations. *Journal of the Atmospheric Sciences*, *59*(3), 590–608. https://doi.org/10.1175/1520-0469(2002)059<0590:VOAAOP>2.0.CO;2

Eckdahl, J. A., Kristensen, J. A., & Metcalfe, D. B. (2022). Climatic variation drives loss and restructuring of carbon and nitrogen in boreal forest wildfire. *Biogeosciences*, *19*(9), 2487–2506. https://doi.org/10.5194/bg-19-2487-2022

Esteve, A. R., Highwood, E. J., Morgan, W. T., Allen, G., Coe, H., Grainger, R. G., et al. (2014). A study on the sensitivities of simulated aerosol optical properties to composition and size distribution using airborne measurements. *Atmospheric Environment*, *89*, 517–524. https://doi.org/10.1016/j.atmosenv.2014.02.063

Feng, Y., Ramanathan, V., & Kotamarthi, V. R. (2013). Brown carbon: A significant atmospheric absorber of solar radiation? *Atmospheric Chemistry and Physics*, *13*(17), 8607–8621. https://doi.org/10.5194/acp-13-8607-2013

Fierce, L., Onasch, T. B., Cappa, D. C., Claudio, M., Swarup, C., Janarjan, B., et al. (2020). Radiative absorption enhancements by black carbon controlled by particle-to-particle heterogeneity in composition. *Proceedings of the National Academy of Sciences USA*, *117*(10), 5196–5203. https://doi.org/10.1073/pnas.1919723117

Filonchyk, M., & Peterson, M. P. (2024). Changes in aerosol properties at the El Arenosillo site in Southern Europe as a result of the 2023 Canadian forest. *Environmental Research*, *260*, 119629. https://doi.org/10.1016/j.envres.2024.119629

Flanner, M. G., Zender, C. S., Randerson, J. T., & Rasch, P. J. (2007). Present-day climate forcing and response from black carbon in snow. *Journal of Geophysical Research*, *112*(D11), D11202. https://doi.org/10.1029/2006JD008003

Fleming, L. T., Lin, P., Roberts, J. M., Selimovic, V., Yokelson, R., Laskin, J., et al. (2020). Molecular composition and photochemical lifetimes of brown carbon chromophores in biomass burning organic aerosol. *Atmospheric Chemistry and Physics*, *20*(2), 1105–1129. https://doi.org/10.5194/acp-20-1105-2020

Folberth, G. A., Hauglustaine, D. A., Lathière, J., & Brocheton, F. (2006). Interactive chemistry in the Laboratoire de Météorologie Dynamique general circulation model: Model description and impact analysis of biogenic hydrocarbons on tropospheric chemistry. *Atmospheric Chemistry and Physics*, *6*, 2273–2319. https://doi.org/10.5194/acp-6-2273-2006

Gillett, N. P., Weaver, A. J., Zwiers, F. W., & Flannigan, M. D. (2004). Detecting the effect of climate change on Canadian forest fires. *Geophysical Research Letters*, *31*(18), L18211. https://doi.org/10.1029/2004gl020876

Grell, G. A., & Freitas, S. R. (2014). A scale and aerosol aware stochastic convective parameterization for weather and air quality modeling. *Atmospheric Chemistry and Physics*, *14*(10), 5233–5250. https://doi.org/10.5194/acp-14-5233-2014

Guang-Ming, W., Zhi-Yuan, C., Shi-Chang, K., Kawamura, K., Ping-Qing, F., Yu-Lan, Z., et al. (2016). Brown carbon in the cryosphere: Current knowledge and perspective. *Advances in Climate Change Research*, *7*(1–2), 82–89. https://doi.org/10.1016/j.accre.2016.06.002

Guenther, A. B., Jiang, X., Heald, C. L., Sakulyanontvittaya, T., Duhl, T., Emmons, L. K., & Wang, X. (2012). The model of emissions of gases and aerosols from nature version 2.1 (MEGAN2.1): An extended and updated framework for modeling biogenic emissions. *Geoscientific Model Development*, *5*(6), 1471–1492. https://doi.org/10.5194/gmd-5-1471-2012

Guo, Z., Yang, Y., Hu, X., Peng, X., Fu, Y., Sun, W., et al. (2022). The optical properties and in-situ observational evidence for the formation of brown carbon in clouds. *Atmospheric Chemistry and Physics*, *22*(7), 4827–4839. https://doi.org/10.5194/acp-22-4827-2022

Gupta, P., Remer, L. A., Levy, R. C., & Mattoo, S. (2018). Validation of MODIS 3 km land aerosol optical depth from NASA's EOS Terra and Aqua missions. *Atmospheric Measurement Techniques*, *11*(5), 3145–3159. https://doi.org/10.5194/amt-11-3145-2018

Gustafsson, O., & Ramanathan, V. (2016). Convergence on climate warming by black carbon aerosols. *Proceedings of the National Academy of Sciences USA*, *113*(16), 4243–4245. https://doi.org/10.1073/pnas.1603570113

Hansen, J., Sato, M., & Reudy, R. (1997). Radiative forcing and climate response. *Journal of Geophysical Research*, *102*, 6831–6864.

Haywood, J., & Boucher, O. (2000). Estimates of the direct and indirect radiative forcing due to tropospheric aerosols: A review. *Reviews of Geophysics*, *38*(4), 513–543. https://doi.org/10.1029/1999RG000078

Heald, C. L., Ridley, D. A., Kroll, J. H., Barrett, S. R. H., Cady-Pereira, K. E., Alvarado, M. J., & Holmes, C. D. (2014). Contrasting the direct radiative effect and direct radiative forcing of aerosols. *Atmospheric Chemistry and Physics*, *14*(11), 5513–5527. https://doi.org/10.5194/acp-14-5513-2014

Hecobian, A., Zhang, X., Zheng, M., Frank, N., Edgerton, E. S., & Weber, R. J. (2010). Water-Soluble Organic Aerosol material and the light-absorption characteristics of aqueous extracts measured over the Southeastern United States. *Atmospheric Chemistry and Physics*, *10*(13), 5965–5977. https://doi.org/10.5194/acp-10-5965-2010

Hems, R. F., Schnitzler, E. G., Bastawrous, M., Soong, R., Simpson, A. J., & Abbatt, J. P. D. (2020). Aqueous photoreactions of wood smoke Brown carbon. *ACS Earth and Space Chemistry*, *4*(7), 1149–1160. https://doi.org/10.1021/acsearthspacechem.0c00117

Hems, R. F., Schnitzler, E. G., Liu-Kang, C., Cappa, C. D., & Abbatt, J. P. D. (2021). Aging of atmospheric Brown carbon aerosol. *ACS Earth and Space Chemistry*, *5*(4), 722–748. https://doi.org/10.1021/acsearthspacechem.0c00346e

Holben, B. N., Tanré, D., Smirnov, A., Eck, T. F., Slutsker, I., Abuhassan, N., et al. (2001). An emerging ground-based aerosol climatology: Aerosol Optical Depth from AERONET. *Journal of Geophysical Research*, *106*(D11), 12067–12097. https://doi.org/10.1029/2001JD900014

Hong, S.-Y., Noh, S.-Y., & Dudhia, J. (2006). A new vertical diffusion package with an explicit treatment of entrainment processes. *Monthly Weather Review*, *134*(9), 2318–2341. https://doi.org/10.1175/MWR3199.1

Hsu, N. C., Tsay, S. C., King, M. D., & Herman, J. R. (2004). Aerosol properties over bright-reflecting source regions. *IEEE Transactions on Geoscience and Remote Sensing*, *42*, 557–569.

Hua, W., Lou, S., Huang, X., Xue, L., Ding, K., Wang, Z., & Ding, A. (2024). Diagnosing uncertainties in global biomass burning emission inventories and their impact on modeled air pollutants. *Atmospheric Chemistry and Physics*, *24*(11), 6787–6807. https://doi.org/10.5194/acp-24-6787-2024

Iacono, M. J., Delamere, J. S., Mlawer, E. J., Shephard, W., Clough, S. A., & Collins, W. D. (2008). Radiative forcing by long-lived greenhouse gases: Calculations with the AER radiative transfer models. *Journal of Geophysical Research*, *113*(D13). https://doi.org/10.1029/2008JD009944

IPCC. (2021). *Climate Change 2021. Physical Science Basis. Contribution of Working Group I to the Sixth Assessment Report of the Intergovernmental Panel on Climate Change*. Cambridge University Press.

Jacobson, M. Z. (2000). A physically-based treatment of elemental carbon optics: Implications for global direct forcing of aerosols. *Geophysical Research Letters*, *27*(2), 217–220. https://doi.org/10.1029/1999GL010968

Jacobson, M. Z. (2001). Global direct radiative forcing due to multicomponent anthropogenic and natural aerosols. *Journal of Geophysical Research*, *106*(D2), 1551–1568. https://doi.org/10.1029/2000jd900514

Jethva, H., & Torres, O. (2019). A comparative evaluation of Aura-OMI and SKYNET near-UV single-scattering albedo products. *Atmospheric Measurement Techniques*, *12*, 6489–6503. https://doi.org/10.5194/amt-12-6489-2019

Jethva, H., Torres, O., & Yoshida, Y. (2019). Accuracy assessment of MODIS land aerosol optical thickness algorithms using AERONET measurements over North America. *Atmospheric Measurement Techniques*, *12*(8), 4291–4307. https://doi.org/10.5194/amt-12-4291-2019

Jimenez, J. L., Canagaratna, M. R., Donahue, N. M., Prevot, A. S. H., Zhang, Q., Kroll, J. H., et al. (2009). Evolution of organic aerosols in the atmosphere. *Science*, *326*(5959), 1525–1529. https://doi.org/10.1126/science.1180353

Jo, D. S., Park, R. J., Lee, S., Kim, S.-W., & Zhang, X. (2016). A global simulation of brown carbon: Implications for photochemistry and direct radiative effect. *Atmospheric Chemistry and Physics*, *16*(5), 3413–3432. https://doi.org/10.5194/acp-16-3413-2016

Kaiser, J. W., Heil, A., Andreae, M. O., Benedetti, A., Chubarova, N., Jones, L., et al. (2012). Biomass burning emissions estimated with a global fire assimilation system based on observed fire radiative power. *Biogeosciences*, *9*(1), 527–554. https://doi.org/10.5194/bg-9-527-2012

Kasthuriarachchi, N. Y., Rivellini, L.-H., Adam, M. G., & Lee, A. K. Y. (2020). Light absorbing properties of primary and secondary Brown carbon in a tropical urban environment. *Environmental Science & Technology*, *54*(17), 10808–10819. https://doi.org/10.1021/acs.est.0c02414

Kaufman, Y. J., Tanré, D., Remer, L. A., Vermote, E. F., Chu, A., & Holben, B. N. (1997). Operational remote sensing of tropospheric aerosol over land from EOS moderate resolution imaging spectroradiometer. *Journal of Geophysical Research*, *102*(D14), 17051–17067. https://doi.org/10.1029/96JD03988

Kirchstetter, T. W., & Thatcher, T. L. (2012). Contribution of organic carbon to wood smoke particulate matter absorption of solar radiation. *Atmospheric Chemistry and Physics*, *12*(14), 6067–6072. https://doi.org/10.5194/acp-12-6067-2012

Kompalli, S. K., Babu, S. S., Ajith, T. C., Moorthy, K. K., Satheesh, S. K., Boopathy, R., et al. (2023). Aging of biomass burning emissions in the Indo-Gangetic Plain outflow: Implications for black carbon light-absorption enhancement. *Atmospheric Research*, *294*, 106949. https://doi.org/10.1016/j.atmosres.2023.106949

Kong, Y., Zhi, G., Jin, W., Zhang, Y., Shen, Y., Li, Z., et al. (2024). A review of quantification methods for light absorption enhancement of black carbon aerosol. *Science of the Total Environment*, *924*, 171539. https://doi.org/10.1016/j.scitotenv.2024.171539

Konovalov, I. B., & Golovushkin, N. A. (2024). Model analysis of origination of semidirect radiative effect of siberian biomass burning aerosol in the Arctic. *Atmospheric and Oceanic Optics*, *37*(3), 382–393. https://doi.org/10.1134/S1024856024700477

Konovalov, I. B., Golovushkin, N. A., & Beekmann, M. (2024). Wildfire-smoke-precipitation interactions in Siberia: Insights from a regional model study. *Science of the Total Environment*, *951*, 175518. https://doi.org/10.1016/j.scitotenv.2024.175518

Konovalov, I. B., Golovushkin, N. A., Beekmann, M., Siour, G., Zhuravleva, T. B., Nasrtdinov, I. M., & Kuznetsova, I. N. (2023). On the importance of the model representation of organic aerosol in simulations of the direct radiative effect of Siberian biomass burning aerosol in the eastern Arctic. *Atmospheric Environment*, *309*, 119910. https://doi.org/10.1016/j.atmosenv.2023.119910

Lack, D. A., Langridge, J. M., Bahreini, R., Cappa, C. D., Middlebrook, A. M., & Schwarz, J. P. (2012). Brown carbon and internal mixing in biomass burning particles. *Proceedings of the National Academy of Sciences USA*, *109*(37), 14802–14807. https://doi.org/10.1073/pnas.1206575109

Lambe, A. T., Cappa, C. D., Massoli, P., Onasch, T. B., Forestieri, S. D., Martin, A. T., et al. (2013). Relationship between oxidation level and optical properties of secondary organic aerosol. *Environmental Science and Technology*, *47*(12), 6349–6357. https://doi.org/10.1021/es401043j

Lan, Z. J., Huang, X. F., Yu, K. Y., Sun, T. L., Zeng, L. W., & Hu, M. (2013). Light absorption of black carbon aerosol and its enhancement by mixing state in an urban atmosphere in South China. *Atmospheric Environment*, *69*, 118–123. https://doi.org/10.1016/j.atmosenv.2012.12.009

Laskin, A., Laskin, J., & Nizkorodov, S. A. (2015). Chemistry of atmospheric Brown carbon. *Chemistry Review*, *115*(10), 4335–4382. https://doi.org/10.1021/cr5006167

Lee, H. J., Aiona, P. K., Laskin, A., Laskin, J., & Nizkorodov, S. A. (2014). Effect of solar radiation on the optical properties and molecular composition of laboratory proxies of atmospheric Brown carbon. *Environmental Science & Technology*, *48*(17), 10217–10226. https://doi.org/10.1021/es502515r

Lesins, G., Chylek, P., & Lohmann, U. (2002). A study of internal and external mixing scenarios and its effect on aerosol optical properties and direct radiative forcing. *Journal of Geophysical Research*, *107*(D10), 4094. https://doi.org/10.1029/2001JD000973

Levy, R., Hsu, C., et al. (2015). MODIS atmosphere L2 aerosol product. In *NASA MODIS Adaptive processing System*. Goddard Space Flight Center. https://doi.org/10.5067/MODIS/MYD04_L2.061

Li, F., Lawrence, D. M., & Bond-Lamberty, B. (2017). Impact of fire on global land surface air temperature and energy budget for the 20th century due to changes within ecosystems. *Environmental Research Letters*, *12*(4), 044014. https://doi.org/10.1088/1748-9326/aa6685

Lin, G., Penner, J. E., Flanner, M. G., Sillman, S., Xu, L., & Zhou, C. (2014). Radiative forcing of organic aerosol in the atmosphere and on snow: Effects of SOA and brown carbon. *Journal of Geophysical Research*, *119*(12), 7453–7476. https://doi.org/10.1002/2013JD021186

Lin, P., Liu, J., Shilling, J. E., Kathmann, S. M., Laskin, J., & Laskin, A. (2015). Molecular characterization of brown carbon (BrC) chromophores in secondary organic aerosol generated from photo-oxidation of toluene. *Physical Chemistry Chemical Physics*, *17*(36), 23312–23325. https://doi.org/10.1039/C5CP02563J

Linares, M., & Ni-Meister, W. (2024). Impact of wildfires on land surface Cold season climate in the northern high-latitudes: A study on changes in vegetation, snow dynamics, albedo, and radiative forcing. *Remote Sensing*, *16*(8), 1461. https://doi.org/10.3390/rs16081461

Liu, D., Whitehead, J., Alfarra, M., reyes-Villegas, E., Spracklen, D. V., Reddington, C. L., et al. (2017). Black-carbon absorption enhancement in the atmosphere determined by particle mixing state. *Nature Geoscience*, *10*(3), 184–188. https://doi.org/10.1038/ngeo2901

Liu, J., Lin, P., Laskin, A., Laskin, J., Kathmann, S. M., Wise, M., et al. (2016). Optical properties and aging of light-absorbing secondary organic aerosol. *Atmospheric Chemistry and Physics*, *16*(19), 12815–12827. https://doi.org/10.5194/acp-16-12815-2016

Liu, P. F., Abdelmalki, N., Hung, H.-M., Wang, Y., Brune, W. H., & Martin, S. T. (2015). Ultraviolet and visible complex refractive indices of secondary organic material produced by photooxidation of the aromatic compounds toluene and m-xylene. *Atmospheric Chemistry and Physics*, *15*(3), 1435–1446. https://doi.org/10.5194/acp-15-1435-2015

Liu, Y., Zhang, K., Qian, Y., Wang, Y., Zou, Y., Song, Y., et al. (2018). Investigation of short-term effective radiative forcing of fire aerosols over North America using nudged hindcast ensembles. *Atmospheric Chemistry and Physics*, *18*(1), 31–47. https://doi.org/10.5194/acp-18-31-2018

Lukács, H., Gelencsér, A., Hammer, S., Puxbaum, H., Pio, C., Legrand, M., et al. (2007). Seasonal trends and possible sources of brown carbon based on 2-year aerosol measurements at six sites in Europe. *Journal of Geophysical Research*, *112*(D23), D23S18. https://doi.org/10.1029/2006JD008151

Luo, J., Zhang, Y., Wang, F., & Zhang, Q. (2018). Effects of brown coatings on the absorption enhancement of black carbon: A numerical investigation. *Atmospheric Chemistry and Physics*, *18*(23), 16897–16914. https://doi.org/10.5194/acp-18-16897-2018

Mailler, S., Menut, L., di Sarra, A. G., Becagli, S., Di Iorio, T., Bessagnet, B., et al. (2016). On the radiative impact of aerosols on photolysis rates: Comparison of simulations and observations in the lampedusa island during the ChArMEx/ADRIMED campaign. *Atmospheric Chemistry and Physics*, *16*(3), 1219–1244. https://doi.org/10.5194/acp-16-1219-2016

Mailler, S., Menut, L., Khvorostyanov, D., Valari, M., Couvidat, F., Siour, G., et al. (2017). CHIMERE-2017: From urban to hemispheric chemistry-transport modeling. *Geoscientific Model Development*, *10*(6), 2397–2423. https://doi.org/10.5194/gmd-10-2397-2017

Menut, L., Bessagnet, B., Briant, R., Cholakian, A., Couvidat, F., Mailler, S., et al. (2021). The CHIMERE v2020r1 online chemistry-transport model. *Geoscientific Model Development*, *14*(11), 6781–6811. https://doi.org/10.5194/gmd-14-6781-2021

Menut, L., Bessagnet, B., Mailler, S., Pennel, R., & Siour, G. (2020). Impact of lightning NOx emissions on atmospheric composition and meteorology in Africa and Europe. *Atmosphere*, *11*(10), 1128. https://doi.org/10.3390/atmos11101128

Menut, L., Cholakian, A., Siour, G., Lapere, R., Pennel, R., Mailler, S., & Bessagnet, B. (2023). Impact of Landes forest fires on air quality in France during the 2022 summer. *Atmospheric Chemistry and Physics*, *23*(13), 7281–7296. https://doi.org/10.5194/acp-23-7281-2023

Menut, L., Flamant, C., Turquety, S., Deroubaix, A., Chazette, P., & Meynadier, R. (2018). Impact of biomass burning on pollutant surface concentrations in megacities of the Gulf of Guinea. *Atmospheric Chemistry and Physics*, *18*(4), 2687–2707. https://doi.org/10.5194/acp18-2687-2018

Menut, L., Schmechtig, C., & Marticorena, B. (2005). Sensitivity of the sandblasting fluxes calculations to the soil size distribution accuracy. *Journal of Atmospheric and Oceanic Technology*, *22*(12), 1875–1884. https://doi.org/10.1175/JTECH1825.1

Meredith, M., et al. (2019). Polar regions. In H.-O. Pörtner, D. C. Roberts, V. Masson-Delmotte, P. Zhai, M. Tignor, E. Poloczanska, et al. (Eds.), *IPCC Special Report on the Ocean and Cryosphere in a Changing Climate*.

Methymaki, G., Bossioli, E., Boucouvala, D., Nenes, A., & Tombrou, M. (2023). Brown carbon absorption in the Mediterranean basin from local and long-range transported biomass burning air masses. *Atmospheric Environment*, *306*, 119822. https://doi.org/10.1016/j.atmosenv.2023.119822

Mie, G. (1908). Beiträge zur Optik trüber Medien, speziell kolloidaler Metallösungen. *Annals of Physics*, *330*(3), 377–445. https://doi.org/10.1002/andp.19083300302

Mischenko, M., Travis, L. D., & Lacis, A. A. (2002). *Scattering, absorption and emission of light by small particles*. Cambridge University Press.

Moise, T., Flores, J. M., & Rudich, Y. (2025). Optical properties of secondary organic aerosols and their changes by chemical processes. *Chemistry Review*, *115*(10), 4400–4439. https://doi.org/10.1021/cr5005259

Monahan, E. C. (1986). The ocean as a source for atmospheric particles. In P. Buat-Ménard (Ed.), *The Role of Air–Sea Exchange in Geochemical Cycling* (pp. 129–163). D. Reidel.

Nenes, A., Pilinis, C., & Pandis, S. (1998). ISORROPIA: A new thermodynamic model for inorganic multicomponent atmospheric aerosols. *Aquatic Geochemistry*, *4*(1), 123–152. https://doi.org/10.1023/A:1009604003981

Neyestani, S. E., & Rawad Saleh, R. (2022). Observationally constrained representation of Brown carbon emissions from wildfires in a chemical transport model. *Environmental Sciences: Atmosphere*, *2*(2), 192–201. https://doi.org/10.1039/D1EA00059D

Palacios-Peña, L., Jiménez-Guerrero, P., Baró, R., Balzarini, A., Bianconi, R., Curci, G., et al. (2019). Aerosol optical properties over Europe: An evaluation of the AQMEII phase 3 simulations against satellite observations. *Atmospheric Chemistry and Physics*, *19*(5), 2965–2990. https://doi.org/10.5194/acp-19-2965-2019

Park, R. J., Kim, M. J., Jeong, J. I., Youn, D., & Kim, S. (2010). A contribution of brown carbon aerosol to the aerosol light absorption and its radiative forcing in East Asia. *Atmospheric Environment*, *44*(11), 1414–1421. https://doi.org/10.1016/j.atmosenv.2010.01.042

Price, C., & Rind, D. (1993). What determines the cloud-to-ground lightning fraction in thunderstorms? *Geophysical Research Letters*, *20*(6), 463–466. https://doi.org/10.1029/93GL00226

Ramnarine, E., Kodros, J. K., Hodshire, A. L., Lonsdale, C. R., Alvarado, M. J., & Pierce, J. R. (2019). Effects of near-source coagulation of biomass burning aerosols on global predictions of aerosol size distributions and implications for aerosol radiative effects. *Atmospheric Chemistry and Physics*, *19*(9), 6561–6577. https://doi.org/10.5194/acp-19-6561-2019

Randerson, J. T., Liu, H., Flanner, M. G., Chambers, S. D., Jin, Y., Hess, P. G., et al. (2006). The impact of boreal forest fire on climate warming. *Science*, *314*(5802), 1130–1132. https://doi.org/10.1126/science.1132075

Rathod, T. D., Sahu, S. K., Tiwari, M., Bhangare, R. C., & Ajmal, P. Y. (2021). Light absorption enhancement due to mixing in black carbon and organic carbon generated during biomass burning. *Atmospheric Pollution Research*, *12*, 101236. https://doi.org/10.1016/j.apr.2021.101236

Remer, L. A., Kaufman, Y. J., Tanré, D., Mattoo, S., Chu, D. A., Martins, J. V., et al. (2005). The MODIS aerosol algorithm, products, and validation. *Journal of the Atmospheric Sciences*, *62*(4), 947–973. https://doi.org/10.1175/JAS3385.1

Riemer, N., Ault, A. P., West, M., Craig, R. L., & Curtis, J. H. (2019). Aerosol mixing state: Measurements, modeling, and impacts. *Reviews of Geophysics*, *57*(2), 187–249. https://doi.org/10.1029/2018RG000615

Romshoo, B., Pöhlker, M., Wiedensohler, A., Pfeifer, S., Saturno, J., Nowak, A., et al. (2022). Importance of size representation and morphology in modelling optical properties of black carbon: Comparison between laboratory measurements and model simulations. *Atmospheric Measurement Techniques*, *15*(23), 6965–6989. https://doi.org/10.5194/amt-15-6965-2022

Saleh, R., Marks, M., Heo, J., Adams, P. J., Donahue, N. M., & Robinson, A. L. (2015). Contribution of brown carbon and lensing to the direct radiative effect of carbonaceous aerosols from biomass and biofuel burning emissions. *J. Geophys. Res.-Atmos.*, *120*(19), 10285–10296. https://doi.org/10.1002/2015JD023697

Schnitzler, E. G., Liu, T., Hems, R. F., & Abbatt, J. P. D. (2020). Emerging investigator series: Heterogeneous OH oxidation of primary brown carbon aerosol: Effects of relative humidity and volatility. *Environmental Science: Processes & Impacts journal*, *22*, 2162–2171. https://doi.org/10.1039/D0EM00311E

Schutgens, N., Dubovik, O., Hasekamp, O., Torres, O., Jethva, H., Leonard, P. J. T., et al. (2021). AEROCOM and AEROSAT AAOD and SSA study – Part 1: Evaluation and intercomparison of satellite measurements. *Atmospheric Chemistry and Physics*, *21*(9), 6895–6917. https://doi.org/10.5194/acp-21-6895-2021

Schwarz, J. P., Gao, R. S., Spackman, J. R., Watts, L. A., Thomson, D. S., Fahey, D. W., et al. (2008). Measurement of the mixing state, mass, and optical size of individual black carbon particles in urban and biomass burning emissions. *Geophysical Research Letters*, *35*(13), L13810. https://doi.org/10.1029/2008GL033968

Seinfeld, J. N., & Pandis, S. N. (2016). *Atmospheric Chemistry and Physics: From Air Pollution to Climate Change* (3th ed.). John Wiley and Sons.

Shiraiwa, M., Kondo, Y., Iwamoto, T., & Kita, K. (2010). Amplification of light absorption of black carbon by organic coating. *Aerosol Science and Technology*, *44*(1), 46–54. https://doi.org/10.1080/02786820903357686

Sinyuk, A., Holben, B. N., Eck, T. F., Giles, D. M., Slutsker, I., Korkin, S., et al. (2020). The AERONET Version 3 aerosol retrieval algorithm, associated uncertainties and comparisons to Version 2. *Atmospheric Measurement Techniques*, *13*(6), 3375–3411. https://doi.org/10.5194/amt-13-3375-2020

Skyllakou, K., Korras-Carraca, M.-B., Matsoukas, C., Hatzianastassiou, N., Pandis, S. N., & Nenes, A. (2024). Predicted concentrations and optical properties of Brown carbon from biomass burning over Europe. *ACS ES&T Air*, *1*(8), 897–908. https://doi.org/10.1021/acsestair.4c00032

Sofiev, M., Ermakova, T., & Vankevich, R. (2012). Evaluation of the smoke-injection height from wild-land fires using remote-sensing data. *Atmospheric Chemistry and Physics*, *12*(4), 1995–2006. https://doi.org/10.5194/acp-12-1995-2012

Soulie, A., Granier, C., Darras, S., Zilbermann, N., Doumbia, T., Guevara, M., et al. (2024). Global anthropogenic emissions (CAMS-GLOB-ANT) for the Copernicus Atmosphere Monitoring Service simulations of air quality forecasts and reanalyses. *Earth System Science Data*, *16*(5), 2261–2279. https://doi.org/10.5194/essd-16-2261-2024

Tanré, D., Kaufman, Y. J., Herman, M., & Mattoo, S. (1997). Remote sensing of aerosol properties over oceans using the MODIS/EOS spectral radiances. *Journal of Geophysical Research*, *102*(D14), 16971–16988. https://doi.org/10.1029/96JD03437

Thompson, G., Field, P. R., Rasmussen, R. M., & Hall, W. D. (2008). Explicit forecasts of winter precipitation using an improved bulk microphysics scheme. Part II: Implementation of a new snow parameterization. *Monthly Weather Review*, *136*(12), 5095–5115. https://doi.org/10.1175/2008MWR2387.1

Toon, O. B., & Ackerman, T. P. (1981). Algorithms for the calculation of scattering by stratified spheres. *Applied Optics*, *20*, 3657–3660. https://doi.org/10.1364/AO.20.003657

Torres, O., Ahn, C., & Chen, Z. (2013). Improvements to the OMI near-UV aerosol algorithm using A-train CALIOP and AIRS observations. *Atmospheric Measurement Techniques*, *6*(11), 3257–3270. https://doi.org/10.5194/amt-6-3257-2013

Torres, O., Decae, R., Veefkind, J. P., & de Leeuw, G. (2002). *OMI aerosol retrieval algorithm, in OMI Algorithm Theoretical Basis Document: Clouds, Aerosols, and Surface UV Irradiance*. version 2 ATBD-OMI-03 (Vol. 3, pp. 47–71). NASA Goddard Space Flight Cent. Retrieved from https://eospso.nasa.gov/sites/default/files/atbd/ATBD-OMI-03.pdf

Torres, O., Tanskanen, A., Veihelmann, B., Ahn, C., Braak, R., Bhartia, P. K., et al. (2007). Aerosols and surface UV products from Ozone Monitoring Instrument observations: An overview. *Journal of Geophysical Research*, *112*(D24), D24S47. https://doi.org/10.1029/2007JD008809

Tuccella, P. (2024). Modelling the black and brown carbon absorption and their radiative impact: The June 2023 intense Canadian boreal wildfires case study. *Retrieved from osf.io/dnygq*.

Tuccella, P., Curci, G., Pitari, G., Lee, S., & Jo, D. S. (2020). Direct radiative effect of absorbing aerosols: Sensitivity to mixing state, brown carbon and dust refractive index and shape. *Journal of Geophysical Research*, *125*(2), e2019JD030967. https://doi.org/10.1029/2019JD030967

Tuccella, P., Menut, L., Briant, R., Deroubaix, A., Khvorostyanov, D., Mailler, S., et al. (2019). Implementation of aerosol-cloud interaction within WRF-CHIMERE online coupled model: Evaluation and investigation of the indirect radiative effect from anthropogenic emission reduction on the Benelux union. *Atmosphere*, *10*(1), 20. https://doi.org/10.3390/atmos10010020

Tuccella, P., Pitari, G., Colaiuda, V., Raparelli, E., & Curci, G. (2021). Present-day radiative effect from radiation-absorbing aerosols in snow. *Atmospheric Chemistry and Physics*, *21*(9), 6875–6893. https://doi.org/10.5194/acp-21-6875-2021

Tuccella, P., Thomas, J. L., Law, K. S., Raut, J.-C., Marelle, L., Roiger, A., et al. (2017). Air pollution impacts due to petroleum extraction in the Norwegian Sea during the ACCESS aircraft campaign. *Elementa: Science of the Anthropocene*, *5*, 25. https://doi.org/10.1525/elementa.124

Updyke, K. M., Nguyen, T. B., & Nizkorodov, S. A. (2012). Formation of brown carbon via reactions of ammonia with secondary organic aerosols from biogenic and anthropogenic precursors. *Atmospheric Environment*, *63*, 22–31. https://doi.org/10.1016/j.atmosenv.2012.09.012

van Bellen, S., Garneau, M., & Bergeron, Y. (2010). Impact of climate change on forest fire severity and consequences for carbon stocks in boreal forest stands of quebec, Canada: A synthesis. *Fire Ecol*, *6*(3), 16–44. https://doi.org/10.4996/fireecology.0603016

Veira, A., Kloster, S., Wilkenskjeld, S., & Remy, S. (2015). Fire emission heights in the climate system – Part 1: Global plume height patterns simulated by ECHAM6-HAM2. *Atmospheric Chemistry and Physics*, *15*(13), 7155–7171. https://doi.org/10.5194/acp-15-7155-2015

Veraverbeke, S., Rogers, B. M., Goulden, M. L., Jandt, R. R., Miller, C. E., Wiggins, E. B., & Randerson, J. T. (2017). Lightning as a major driver of recent large fire years in North American boreal forests. *Nature Climate Change*, *7*(7), 529–534. https://doi.org/10.1038/nclimate3329

Walker, J. X., Rogers, B. M., Baltzer, J. L., Cumming, S. G., Day, N. J., Goetz, S. J., et al. (2018). Cross-scale controls on carbon emissions from boreal forest megafires. *Global Change Biology*, *24*(9), 4251–4265. https://doi.org/10.1111/gcb.14287

Wang, J., Wang, J., Cai, R., Liu, C., Nie, W., Wang, J., et al. (2023). Unified theoretical framework for black carbon mixing state allows greater accuracy of climate effect estimation. *Nature Communications*, *14*(1), 2703. https://doi.org/10.1038/s41467-023-38330-x

Wang, X., Heald, C. L., Liu, J., Weber, R. J., Campuzano-Jost, P., Jimenez, J. L., et al. (2018). Exploring the observational constraints on the simulation of brown carbon. *Atmospheric Chemistry and Physics*, *18*(2), 635–653. https://doi.org/10.5194/acp-18-635-2018

Wang, X., Heald, C. L., Ridley, D. A., Schwarz, J. P., Spackman, J. R., Perring, A. E., et al. (2014). Exploiting simultaneous observational constraints on mass and absorption to estimate the global direct radiative forcing of black carbon and brown carbon. *Atmospheric Chemistry and Physics*, *14*(20), 10989–11010. https://doi.org/10.5194/acp-14-10989-2014

Wang, X., Heald, C. L., Sedlacek, A. J., de Sá, S. S., Martin, S. T., Alexander, M. L., et al. (2016). Deriving brown carbon from multiwavelength absorption measurements: Method and application to AERONET and aethalometer observations. *Atmospheric Chemistry and Physics*, *16*(19), 12733–12752. https://doi.org/10.5194/acp-16-12733-2016

Wang, X., Zhang, L., & Moran, M. D. (2014). Development of a new semi-empirical parameterization for below-cloud scavenging of size-resolved aerosol particles by both rain and snow. *Geoscientific Model Development*, *7*(3), 799–819. https://doi.org/10.5194/gmd-7-799-2014

Wang, Y., Li, W., Huang, J., Liu, L., Pang, Y., He, C., et al. (2021). Nonlinear enhancement of radiative absorption by black carbon in response to particle mixing structure. *Geophysical Research Letters*, *48*(24), e2021GL096437. https://doi.org/10.1029/2021GL096437

Wesely, M. (1989). Parameterization of surface resistances to gaseous dry deposition in regional-scale numerical models. *Atmospheric Environment*, *23*(6), 1293–1304. https://doi.org/10.1016/0004-6981(89)90153-4

Wild, O., Zhu, X. P., & Fast-J, M. J. (2000). Accurate simulation of in- and below-cloud photolysis in tropospheric chemical models. *Journal of Atmospheric Chemistry*, *37*, 245–282. https://doi.org/10.1023/A:1006415919030

Xu, L., Lin, G., Liu, X., Wu, C., Wu, Y., & Lou, S. (2024). Constraining light absorption of brown carbon in China and implications for aerosol direct radiative effect. *Geophysical Research Letters*, *51*(16), e2024GL109861. https://doi.org/10.1029/2024GL109861

Yus-Díez, J., Via, M., Alastuey, A., Karanasiou, A., Minguillón, M. C., Perez, N., et al. (2022). Absorption enhancement of black carbon particles in a mediterranean city and countryside: Effect of particulate matter chemistry, ageing and trend analysis. *Atmospheric Chemistry and Physics*, *22*(13), 8439–8456. https://doi.org/10.5194/acp-22-8439-2022

Zeng, L., Tan, T., Zhao, G., Du, Z., Hu, S., Shang, D., & Hu, M. (2024). Overestimation of black carbon light absorption due to mixing state heterogeneity. *npj Climate and Atmospheric Science*, *7*(1), 2. https://doi.org/10.1038/s41612-023-00535-8

Zhang, A., Wang, Y., Zhang, Y., Weber, R. J., Song, Y., Ke, Z., & Zou, Y. (2020). Modeling the global radiative effect of brown carbon: A potentially larger heating source in the tropical free troposphere than black carbon. *Atmospheric Chemistry and Physics*, *20*(4), 1901–1920. https://doi.org/10.5194/acp-20-1901-2020

Zhang, L., Gong, S., Padro, J., & Barrie, L. (2001). A size-segregated particle dry deposition scheme for an atmospheric aerosol module. *Atmospheric Environment*, *35*(3), 549–560. https://doi.org/10.1016/S1352-2310(00)00326-5

Zhang, Y., Favez, O., Canonaco, F., Liu, D., Močnik, G., Amodeo, T., et al. (2018). Evidence of major secondary organic aerosol contribution to lensing effect black carbon absorption enhancement. *npj Climate and Atmospheric Science*, *1*, 47. https://doi.org/10.1038/s41612-018-0056-2

Zhang, Y., Forrister, H., Liu, J., Dibb, J., Anderson, B., Schwarz, J. P., et al. (2017). Top-of-atmosphere radiative forcing affected by brown carbon in the upper troposphere. *Nature Geoscience*, *10*(7), 486–489. https://doi.org/10.1038/ngeo2960

Zhao, G., Tan, T., Zhu, Y., Hu, M., & Zhao, C. (2021). Method to quantify black carbon aerosol light absorption enhancement with a mixing state index. *Atmospheric Chemistry and Physics*, *21*(23), 18055–18063. https://doi.org/10.5194/acp-21-18055-2021

Zhao, R., Lee, A. K. Y., Huang, L., Li, X., Yang, F., & Abbatt, J. P. D. (2015). Photochemical processing of aqueous atmospheric brown carbon. *Atmospheric Chemistry and Physics*, *15*(11), 6087–6100. https://doi.org/10.5194/acp-15-6087-2015

Zhong, M., & Jang, M. (2014). Dynamic light absorption of biomass-burning organic carbon photochemically aged under natural sunlight. *Atmospheric Chemistry and Physics*, *14*(3), 1517–1525. https://doi.org/10.5194/acp-14-1517-2014